BL1A

# Mo $L_3$-XANES Study of Silylation Effect for Methane Dehydroaromatization over Mo/H-MFI Catalysts

H. Aritani, K. Kuramochi and S. Yoshinaga
*Faculty of Engineering, Saitama Institute of Technology, Fukaya 369-0293, Japan*

A Mo-modified H-MFI zeolite (Mo/H-MFI) catalyst is one of a typical catalyst for direct GTL (Gas to liquid), because it shows high activity for dehydroaromatization of methane in absence of oxygen. In this reaction, reduction of Mo species is brought about in contact with methane in initial step, and reduced Mo ions react methane to form carbide and/or oxycarbide species in next step. It has been accepted that the carbide and/or oxycarbide species are the active center for dehydroaromatization of methane. However, deactivation cannot be avoided by carbon deposition. Hydrogen co-feed with methane is one of an effective method for suppression of coking. However, excess hydrogen may affect a reduction of Mo species during the reaction, and decrease of active Mo-oxycarbide species may give low reactivity. On the other hand, strong acid sites in external H-MFI surface possibly relates to the coking directly. Thus, selective covering of the coking site may be effective for durable activity [1]. Silylation of one of a unique method for selective coverage of external acid sites onto H-MFI. This study focused on the effect of silylation on methane dehydroaromatization over Mo/H-MFI catalysts. Mo $L_{III}$-edge XANES studies were introduced to characterize the active Mo species on bare and silylated H-MFI.

Catalysts were prepared by impregnation of H-MFI ($Si/Al_2$=67) synthesized hydrothermally with $MoO_2(acac)_2$–$CHCl_3$ solution, and followed by drying overnight and calcination at 773 K. $MoO_3$-loading amount is 5.0 wt% in whole catalysts. For silylation of Mo/H-MFI catalysts, heptane solution of teiethoxyvinylsilane (Mo/Si=10) was employed for impregnation, and followed by drying and calcination at 873 K. Mo $L_{III}$-edge XANES spectra were operated in BL1A of UVSOR-IMS in a top-up mode. InSb double crystal monochromator was used for the XANES measurements in a total-electron yield mode. The value of photon energy was calibrated by using Mo metal-foil at Mo $L_{III}$-edge, and normalized XANES spectra and their second derivatives were obtained for characterization. Catalytic activity was evaluated in a fixed bed flow reactor. Each catalyst (0.250 g) was placed in a quartz-tube reactor, and pretreated in He–CO(0-2%) flow (30 mL $min^{-1}$) at 973 K for 1 h. Then $CH_4$(20%)– $H_2$(1%)–He reactant gas was fed at 973 K (30 mL $min^{-1}$: SV = 7.2 L $g^{-1}$ $h^{-1}$). Products were analyzed by online GC.

Figure 1 shows the Mo $L_{III}$-XANES spectra of silylated/unsilylated Mo/H-MFI catalysts after dehydroaromatization at 973 – 1073 K for 3 h. As

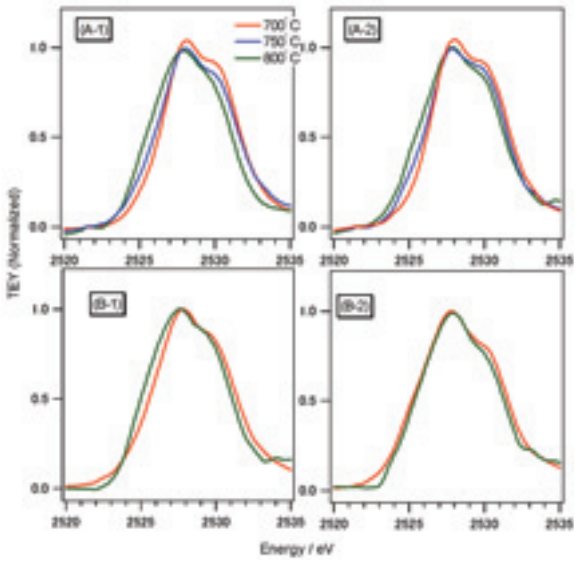


Fig. 1. Mo $L_{III}$-edge XANES spectra of (A) bare- and (B) Silylated- $MoO_3$(5.0wt%)/H-MFI catalysts after methane dehydroaromatization with (1) $CH_4$(20%)-He or (2) $CH_4$(20%)-$H_2$(1.0%)-He at various reaction temperature.

shown in Fig. 1 (A-1 and B-1), According to a higher reaction temperature, the edge energy of XANES threshould becomes lower. It indicates the reduction and/or carbonization of $MoO_x$ species to $MoO_xC_y$ ones. Excess reduction of Mo species brings about the deactivation of the catalysts because of excess carbon deposition [1, 2]. In case of silylated Mo/H-MFI [Fig. 1 (B-1) and (B-2)], the reduction degree of Mo species is almost as same as bare Mo/H-MFI [Fig. 1 (A-1) and (A-2)]. On these catalysts, high and durable activity for methane dehydroaromatization is significantly shown by silylation. The effect of silylation is possibly due to the depression of coking from methane, and the reduction of Mo species is almost independent. For Mo/H-MFI catalysts, formation of active $MoO_xC_y$ species (partially carbonized $MoO_x$) is one of a key role for high activity. And thus, deactivation of coking sites in H-MFI extrapores is very effective to obtain durable activity. In this study, it is suggested that silylation by using teiethoxyvinylsilane act as the depression of activity on the coking sites because coking amount becomes low. Detailed study about the silylation effect on Mo species is now in progress.

[1] H. Aritani, S. Shinohara, S. Koyama, K. Otsuki, T. Kubo, A. Nakahira, Chem. Lett. **35** (2006) 416.
[2] H. Aritani, H. Shibasaki, H. Orihara, A. Nakahira, J. Environm. Sci. **21-6** (2009) 736.

BL1A

# XANES Analysis of Na-Incorporated β-Tricalcium Phosphate

K. Kawabata[1] and T. Yamamoto[2]

[1]*Department of Holistic Human Science, Kwansei Gakuin University, 662-8501, Japan*

[2]*Faculty of Science and Engineering, WasedaUniversity, 169-8555, Japan*

Bioceramics based on the calcium phosphate are now widely used for repairing the bone defects. As it is well known that the main component of the inorganic part of human bone consists of hydroxyapatite (HAp). HAp itself is, of course, used as bioceramics, but other calcium phosphates are also employed, in which β-tricalcium phosphate (β-TCP) is one of the most active one. It was reported that incorporation of trace elements in such bioceramics accelerates the creation of HAp in the human body. To understand the influence of trace elements, it is essential to understand the local environment of trace elements in an atomic scale. We have systematically investigated the local environment of divalent ions, i.e., $Mg^{2+}$ [1], $Mn^{2+}$ [2] and $Zn^{2+}$ [3], by the XANES measurements with the aid of the first-principles calculations. In the present study, local environment of monovalent Na ions in β-TCP is investigated by the Na-K XANES measurements.

Sample specimens were fabricated by the conventional solid-state reaction method. High purity powders of $CaHPO_4$, $CaCO_3$ and $NaHCO_3$ were mixed and ground in an agate mortar, which were calcined at 1273 K for 6 hours in air. Na-K XANES spectra are measured at BL1A in UVSOR by the total electron yield method. Sample powders were mounted on the first dinode of the electron multiplier using the carbon adhesive tape.

Observed Na-K XANES spectrum of Na-incorporated β-TCP is shown in Fig. 1 together with that of NaCl for comparison. It is difficult to determine the local environment of Na ions in β-TCP only from the comparison with the spectra of standard materials. Then the theoretical calculations are mandatory for the quantitative analysis of the local environment of incorporated Na ions. Here the first-principles calculations were carried out to obtain the theoretical Na-K XANES spectra of Na in β-TCP by using the WIEN2k package [4], in which the core-hole effect was directly included by removing the Na 1s electron. Several models by changing the substituted sites of Na incorporation were constructed. Calculated spectrum using the model, in which Na is substituted at Ca(4) site in β-TCP, is compared with the observed one in Fig. 2. Observed Na-K XANES profile of Na-incorporated β-TCP is quantitatively well reproduced by this model. This result confirmed that the incorporated Na ions are substituted at Ca(4) site in β-TCP.

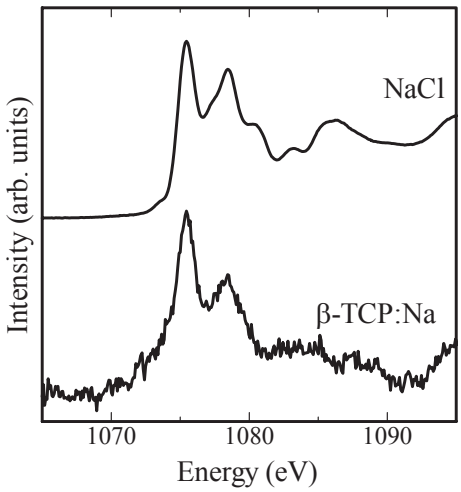


Fig. 1. Observed Na-K XANES spectra of Na-incorporated β-TCP ($Ca_{2.7}Na_{0.3}(PO_4)_2$) and NaCl.

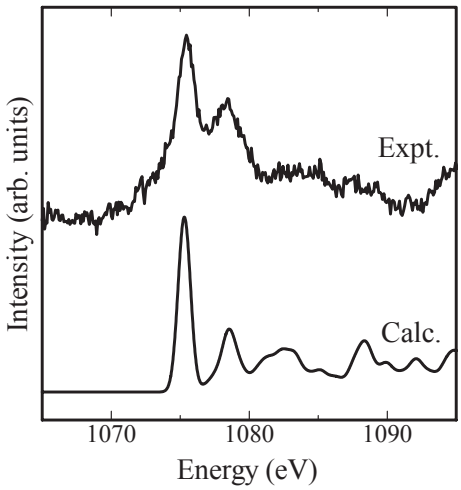


Fig. 2. Comparison between observed and calculated Na-K XANES spectra of Na-incorporated β-TCP.

[1] K. Kawabata, H. Sato and T. Yamamoto, UVSOR Activity Report **35** (2007) 108.
[2] K. Kawabata, H. Sato and T. Yamamoto, J. Ceram. Soc. Jpn. **116** (2008) 108.
[3] K. Kawabata, T. Yamamoto and A.Kitada, Physica B **406** (2011) 890.
[4] http://www.wien2k.at

BL1A

# Evaluation of Hydrotalcite-Based Nanosheet by Soft Chemical Process

A. Nakahira[1], S. Yamamoto[1], M. Sato[2], Y. Takamatsu[1], S. Misu[1] and H. Aritani[3]

[1]*Faculty of Engineering, Osaka Prefecture University, Gakuencho, Sakai 599-8531, Japan*

[2]*Osaka Center, IMR, Tohoku University, Gakuencho, Sakai 599-8531, Japan*

[3]*Saitama Institute of Technology, Fukaya 369-0293, Japan*

## Introduction

Layered double hydroxide (LDH) is one of unique clay minerals with a layered structure, its composition formula of $[M^{2+}_{1-X}\ M^{3+}_{X}\ (OH)_2 \cdot A^{n-}_{X/n} \cdot nH_2O]$. These LDH and its related materials are expected to be one of novel materials because of their potential applications in wide areas, such as catalysis, adsorption, and nanocomposite and drug delivery. Recently, the nanosheets from the exfoliation of layered host compounds have received increasing attention because the resulting unilamellar materials or nanosheets have various attractive aspects. Furthermore, the nanosheets from the LDH are expected to be especially useful among novel nanosheet related materials.

In the present study, we focused on the structural evaluation of the nanosheets from LDH basically composed of $Mg^{2+}$ and $Al^{3+}$, which is called hydrotalcite, "MgAl-Tal". Furthermore, it is known that these nanosheets are important for the novel nanostructured materials synthesized by the layer-by-layer methods. However, it is not clarified about the detailed structure evaluation of the nanosheets from MgAl-Ta. In the present study, the structure evaluation of the nanosheets from LDH composed of $Mg^{2+}$ and $Al^{3+}$ (MgAl-Tal: hydrotalcite) were performed.

## Experiments

From 0.2 mol/dm$^3$ $MgCl_2$ aqueous solution and 0.1 mol/dm$^3$ $AlCl_3$ aqueous solution, mixing solution was prepared by the co-precipitation method. MgAl-Tal with $M^{2+}/M^{3+}$ =2~4 were synthesized by adding mixing solution into 0.05 mol/dm$^3$ $NaHCO_3$ at room temperature. 1 mol/dm$^3$ NaOH was simultaneously added into the aqueous solution in order to keep pH 10. Products for MgAl-Tal were aged at room temperature for 2 hours. They were separated and sufficiently washed by deionized water and finally air-dried at 50 ℃ for 24 hours. The delamination of obtained MgAl-Tal products were prepared by soft chemical process. The products were obtained from the delamination of MgAl-Tal.

The local structures around Al for the nanosheets were characterized by measuring X-ray adsorption near edge structure (XANES) at BL1A in UVSOR with KTP.

## Results and Discussion

MgAl-Tal samples prepared by the co-precipitation method was identified to be a layered double hydroxide consisted of $Mg^{2+}$ and $Al^{3+}$ by powder X-ray diffraction analysis. Then, the delamination of obtained products were successfully prepared by the soft chemical process. The products obtained from the delamination of MgAl-Tal indicated the tyndall phenomenon, suggesting that nanosheets were obtained. It was suggested that products obtained from the delamination of MgAl-Tal had broad peaks derived from XRD results.

Figure 1 shows the results of XANES of Al-*K* edge of the nanosheet products obtained from the delamination of MgAl-Tal. For the comparison, MgAl-Tal samples prepared by the co-precipitation method were similarly evaluated. The spectrum of he nanosheet products obtained from the delamination of MgAl-Tal corresponded approximately to that of MgAl-Tal samples prepared by the co-precipitation. It was elucidated that Al-K edge XANES spectra of the nanosheet products obtained from the delamination of MgAl-Tal were similar to that of MgAl-Tal as a starting material.

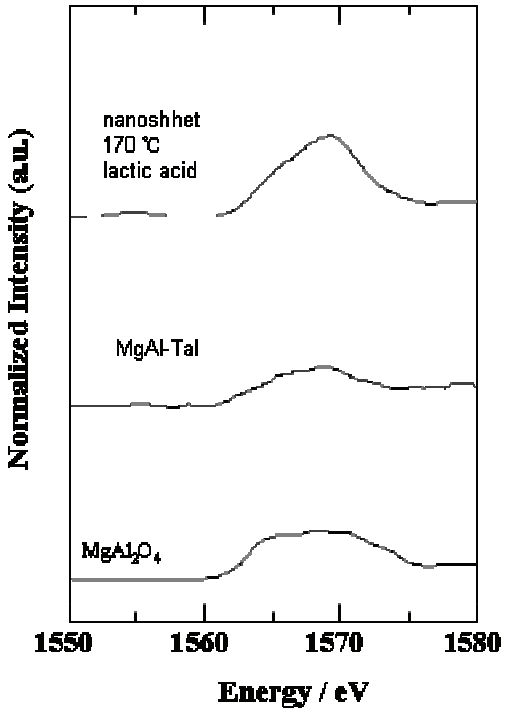


Fig. 1. Results of XANES of Al-*K* edge of the MgAl-Tal nanosheet.

BL1A

# Evaluation of Local Structure of SBF-Type Mesoporous Silica Bulks

A. Nakahira[1,2], S. Yamamoto[1], M. Sato[2], Y. Takamatsu[1], S. Misu[1], Y. Kawabe[1], Y. Nishio[1] and H. Aritani[3]

[1]*Faculty of Engineering, Osaka Prefecture University, Gakuencho, Sakai 599-8531, Japan*
[2]*Osaka Center, IMR, Tohoku University, Gakuencho, Sakai 599-8531, Japan*
[3]*Saitama Institute of Technology, Fukaya 369-0293, Japan*

## Introduction

Much attention has been paid to the mesoporous silica families, MCM, FSM, and SBF and so on. Since SBA-15 powders synthesized by the sol-gel method with triblock copolymer surfactants possess a huge specific surface area and range of relatively uniform pore size and furthermore contain a unique internal structure with uniform arrays of hexagonal mesopore, it is expected to be potentially useful as catalysts supports and adsorbent and so on. In particular, SBA-15 powders have the thicker silica walls around mesopores than that of MCM-type mesoporous silica (MCM and FSM) made with conventional cationic surfactants, leading to the stability for SBA-15 at high temperature and/or under severe conditions. However, the development for the preparation of bulky mesoporous silica SBA-15 is strongly desired, because powdered SBA-15 materials are restricted in their practical application in many fields. We successfully prepared the dense SBA-15 bulk by the modified hydrothermal hot-pressing process. In this study, the local structures for SBF-type mesoporous silica bulks were investigated by XAFS measurements.

In the present study, we focused on the structure evaluation of the bulks of SBF-type mesoporous silica by the modified hydrothermal hot-pressing process. In special, the structure evaluations of the SBF-type bulk were performed.

## Experiments

SBA-15 was synthesized by the following method. Silica and block copolymer mesophases were synthesized at room temperature as follows. Pluronic P123 ($M_{av}$=5800, EO20PO70EO20) as a block copolymer was dissolved in water and HCl solution with stirring at room temperature. Then, TEOS as a silica was added into that solution with stirring at room temperature. The mixture was aged at 80 ºC for 12 h without stirring. The solid product was filtered, washed, and air-dried at room temperature. Calcination was carried out, slowly increasing temperature from room temperature to 500 ºC and heating at 500 ºC for 6 hours. Subsequently, the consolidation of this SBA-15 powder was carried out by the modified thermal hot pressing method with the uniaxial pressure of 30 MPa at 110 ºC to 150 ºC for 2 h. After the modified thermal hot pressing treatments, obtained bulks were heat-treated at 600 ºC in the air atmosphere. The local structures around Si for the products of SBF-type bulk were characterized by measuring X-ray adsorption near edge structure (XANES) at BL1A in UVSOR.

## Results and Discussion

Dense SBA-15 bulks were successfully synthesized by the modified hydrothermal hot-pressing possess. These dense SBA-15 bulks with mesoporous structure were similar to that of powdered SBA-15, suggesting that the dense SBA-15 bulks with mesoporous structure as well as powdered SBA-15 were successfully synthesized by the modified hydrothermal hot-pressing possess.

Figure 1 shows the results of X-ray adsorption near edge structure (XANES), Si-K edge, for SBA-15 bulk prepared by the modified hydrothermal hot-pressing at 150 ºC. For the comparison, $SiO_2$, FSM and SBA-15 powder were similarly evaluated. X-ray adsorption near edge structure (XANES) of the dense SBA-15 bulks indicated the similar pattern of powdered SBA-15. It was obvious that dense SBA-15 bulks obtained by the hydrothermal hot-pressing possess hexagonal regularity similar to powdered SBA-15 from these Si-K edge XANES results.

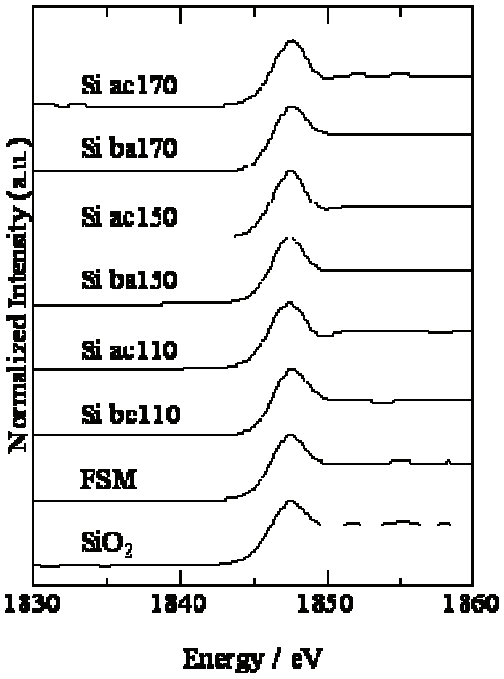


Fig. 1. The results of X-ray adsorption near edge structure (XANES), Si-K edge, for SBA-15 bulks.

BL1A

# Investigation of Local Structure of Mg K-Edge in Chitosan and Mg Co-Addition Calcium Phosphate Materials

T. Onoki[1], Y. Nishio[1], T. Moriguchi[1], Y. Kawabe[1], M. Sato[2] and A. Nakahira[1,2]

[1]*Graduate School of Engineering, Osaka Prefecture University, Sakai 599-8531, Japan*

[2]*Osaka Center for Industrial Materials Research, Institute for Materials Research, Tohoku University, Sakai 599-8531, Japan*

Human bone has an organic/inorganic composite structure. Bone replacing biomedical materials, for example hydroxyapatite (HA) ceramics, has been required more biocompatibility and optimal mechanical properties. Recently, bioceramics were fabricated by some hydrothermal techniques at low temperature [1]. Magnesium (Mg) is known to be an important trace element in bone and teeth. Indeed, despite its low concentration (generally between 0.5 and 1.5 wt%), it plays a key role in bone metabolism, in particular during the early stages of osteogenesis where it stimulates osteoblast proliferation, and its depletion causes bone fragility and bone loss. Relationships have been suggested between the magnesium content in enamel and the development of dental caries. Given the biological relevance of magnesium, many research teams have worked on the preparation of apatite and calcium phosphate implant materials containing relatively low levels of Mg, which has been shown to improve their bioactivity [2]. According to the literature, the replacement of calcium by magnesium in HA is difficult.

Chitosan was one of origanic materials derived from crab shell. And has function of accumulating mineral species. So we conducted for making a Mg adding HA/chitosan composite ceramic for more biocompatibility. Calcium hydrogen phosphate di-hydrate (DCPD) is one of starting materials for HA ceramics through a hydrothermal hot-pressing technique at around 100 ºC [1]. As a first step, Mg adding DCPD/chitosan composite powder were prepared. Co-precipitation method was employed in order to prepare Mg adding DCPD/chitosan composite materials. The composite materials were based on the DCPD preparation [3], which 1.0*M* calcium nitrate solution (99.0%; $Ca(NO_3)_2 \cdot 4H_2O$, KANTO CHEMICAL, Japan) and 1.0*M* di-ammonium hydrogen phosphate solution (98.5%; $(NH_4)_2HPO_4$ ; KANTO CHEMICAL, Japan) were mixed. Magnesium chloride (99.0%; MgCl; Wako, Japan) Chitosan powder (LLWP Grade, KIMICA, Japan) was dissolved in water with a little acetic acid. The chitosan and MgCl solution was added to $Ca(NO_3)_2 \cdot 4H_2O$ solution with various concentration before mixing to the $(NH_4)_2HPO_4$ solution. And then the fabricated powder were converted to HA by a hydrothermal treatment (150 ºC, 2h).

Mg K-edge XANES spectra for the fabricated powders were obtained in a total electron yield mode at room temperature using a KTP double-crystal monochrometer at BL1A station of UVSOR. The spectra were collected in the photon energy range from 1295-1330 eV at intervals of 0.05eV with a dwell time of 1s. Mg-K edge XANES of the DCPD/chitosan composite and the HA converted powder were shown in Figure 1. Firstly, we could not detect Mg in the HA sample without chitosan. On the other hand, a little amount of Mg can be observed in both of DCPD and HA with chitosan. These result indicate that chitosan play an important role for Mg adding to calcium phosphate materials. It is shown that chitosan is a good carrier for doping non-HA mineral elements to HA.

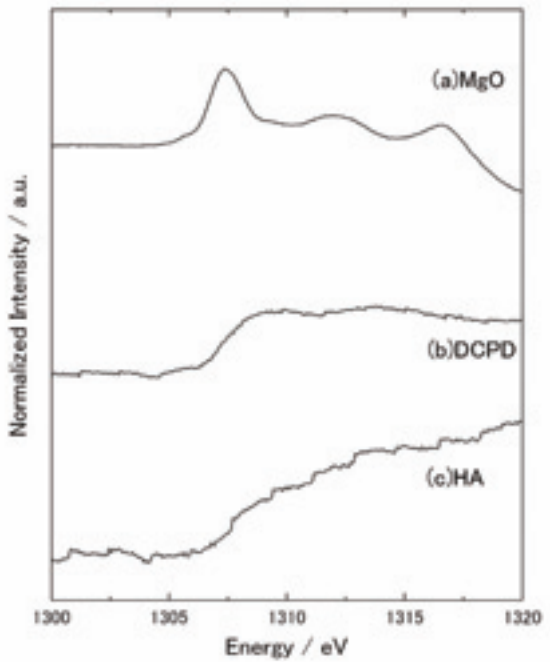


Fig. 1. XANES spectra of Mg K-edge of the DCPD/chitosan composite and the HA converted powder with Mg.

[1] S. Ishihara, T. Matsumoto, T. Onoki, T. Sohmura and A. Nakahira, Mater. Sci. Eng. C **29** (2009) 1885.
[2] S. Gomes, G. Renaudin, E. Jallot and J. M. Nedelec, ACS Appl. Mater. Interfaces **1** (2009) 505.
[3] T. Onoki, K. Hosoi and T. Hashida, Scr. Mater. **52** (2005) 767.

BL1A

# Investigation of Effect of Ions in Seawater for Ettringite Formation

M. Sato[1], S. Yamamoto[2], Y. Nishio[2], Y. Takamatsu[2] K. Kumadani[2] and A. Nakahira[1,2]

[1]*Osaka Center for Industrial Materials Research, Tohoku University, Sakai 599-8531, Japan*

[2]*Graduate School of Engineering, Osaka Prefecture University, Sakai 599-8531, Japan*

Ettringite ($3CaO \cdot Al_2O_3 \cdot 3CaSO_4 \cdot 32H_2O$) is one of calcium sulpho aluminate (CSA) system, and it has a needle-like microstructure belongs to hexagonal system. It is a naturally occurring mineral found in Germany for the first time. This mineral is characterized by the very high content of water molecules. Since ettringite is important material to provide the rapid set and/or high early strength for constructional materials, more effective material design can be expected by investigating the generation behavior in detail. However, there are few reports for the generative mechanism of ettringite. In this study, we prepared ettringite using different aqueous solutions including $Mg^{2+}$, $Na^{+}$, $CO_3^{2-}$, $SO_4^{2-}$ ions etc. and investigated the generation behavior in different ion enviroments.

In order to obtain the ettringite, tricalcium aluminate (C3A, $3CaO \cdot Al_2O_3$) were firstly prepared by $CaCO_3$ and $Al_2O_3$ powders as starting materials. After mixed up each powder, it was calcinated at 1573 K for 36 hours in air. And then, obtained C3A and $CaSO_4 \cdot 2H_2O$ were mixed and stirred at 200 rpm from 5 minutes to 24 hours in the different aqueous solutions. After stirring, samples were filtered and dried.

Na-K, Mg-K, Al-K and S-K edge XANES spectra of obtained ettringite powders were measured in a total electron yield mode at room temperature using Beryl, KTP and InSb double-crystal monochrometer at BL1A station of UVSOR, respectively.

Figure 1 shows Mg-K edge XANES spectra of ettringite prepared in 1 mol/l $MgCl_2$ aqueous solution at room temperature for several aging times. In the case of $MgCl_2$ solution with 0.01 mol/l concentration, no peaks derived from Mg compounds were observed. However, spectra derived from Mg compounds were observed in the case of 0.1 and 1 mol/l MgCl solution as shown in Fig. 1. From XANES measurement, it is suggested that the Mg based layered double hydroxide (LDH) is generated within 5 minutes, and the generation of LDH affects the formation of ettringite. Similar trend that the ettringite formation is affected at the concentration of solution more than 0.1 mol/l was obtained in other solution such as NaCl, KCl and $Na_2SO_4$.

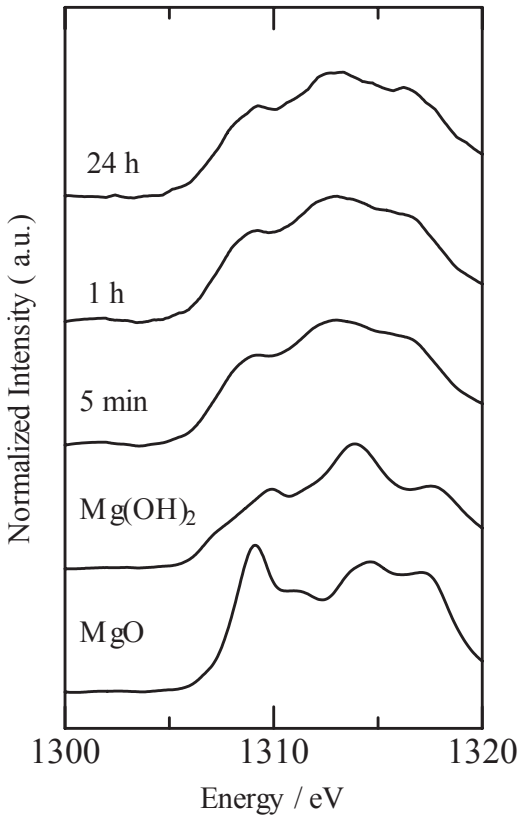


Fig. 1. Mg-K edge XANES spectra of ettringite prepared in 1 mol/l $MgCl_2$ aqueous solution at room temperature for several aging times.

BL1A

# Investigation of Local Structure of P-K Edge in Fe Doped HAp

M. Sato[1], S. Yamamoto[2], Y. Nishio[2], Y. Takamatsu[2] and A. Nakahira[1,2]

[1]*Osaka Center for Industrial Materials Research, Tohoku University, Sakai 599-8531, Japan*

[2]*Graduate School of Engineering, Osaka Prefecture University, Sakai 599-8531, Japan*

So far, many kinds of magnetic beads such as paramagnetic iron oxide particles and surface-modified ones by polymer have been widely used in a medical field. However, those iron oxide based magnetic beads have been pointed out the risk of the elution of iron by long term use. The resolvability of iron strongly depends on its particle size. Since the particle size of magnetic beads is decided by a service space, control of resolvability is one of the problems that we should overcome to use it in a living body. Because the elution of iron affects proliferation and metabolism of cell, there is a possibility to exhibit some toxicity. Therefore, development of non toxic magnetic bead has been strongly desired. Hydroxyapatite ($Ca_{10}(PO_4)_6(OH)_2$, HAp) is a good candidate for drug delivery system materials due to its excellent ion exchange ability and protein adsorption ability. By using these unique abilities of HAp, non toxic magnetic bead can be developed.

In this study, Fe doped HAp was prepared by conventional wet process and local structure around P atom was investigated by XAFS measurement.

0.1 mol/l $Ca(NO_3)_2$, $(NH_4)_2HPO_4$ and $FeCl_3$ solutions were used as starting materials. These solutions were mixed up each other becoming the ratio of Ca to P of 1.67 and the ratio of Fe from 0 to 20 mol% for Ca solution. Mixed solution was aged for 1 h at room temperature and then it was filtered and dried at 323 K for overnight. P-K edge XANES spectra of Fe doped HAp powders were measured in a total electron yield mode at room temperature using InSb double-crystal monochrometer at BL1A station of UVSOR.

Figure 1 shows P-K edge XANES spectra of Fe doped HAp prepared by conventional wet process at room temperature. Obtained P-K edge XANES spectra of samples were similar to that of commercial HAp, and a change of the spectral pattern was not clearly observed within any ratio of Fe. This result indicates that the local structure of around P atom of Fe doped HAp samples is almost same with commercial HAp.

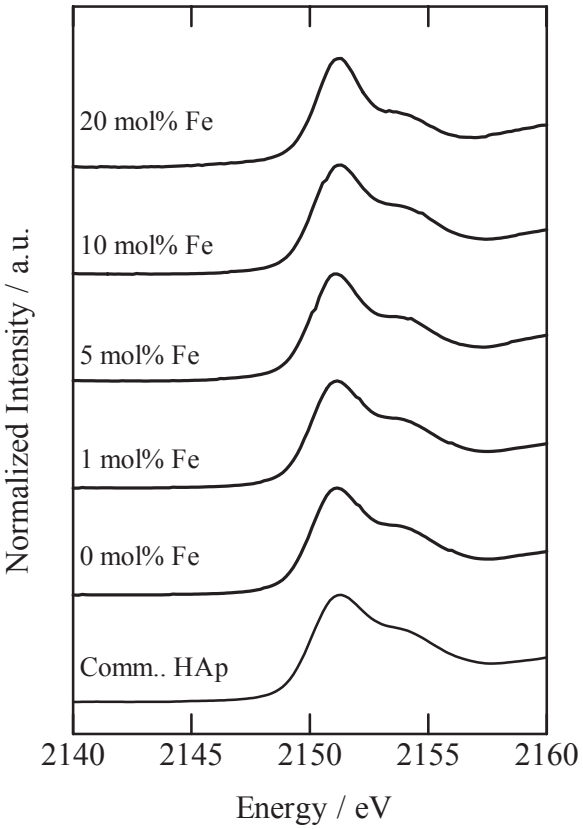


Fig. 1. P-K edge XANES spectra of Fe doped HAp prepared by conventional wet process at room temperature.

BL1B

# Optical Spectroscopy of ZnO Thin Films

N. Kashiwagura, Y. Kubo, T. Hashida, Y. Hayashi and M. Yamaga
*Department of Mathematical and Design Engineering, Gifu University, Gifu 501-1193, Japan*

Today the most widely adopted TCO (Transparent Conductive Oxides) films for use as electrodes of solar cell and liquid crystal display is ITO (Indium Tin Oxides) films. However, ITO films include so sparse Indium that the substitutive materials are expected. ZnO thin films are one of the hopeful materials as TCO films.

ZnO thin films were deposited on a fused silica glass (10 mm x 20 mm x 0.5 mm) by the DC sputtering method. The sputtering time, the gas (Ar) pressure and the substrate temperature were 240 minutes, 0.40 Torr. and 200 ℃, respectively. The induced electric power was 60 W for sample 1, and 45 W for sample 2.

Optical absorption, luminescence and excitation spectra were measured using the BL1B beam in the temperature range of 10-300 K.

Figure 1 shows the optical absorption spectra for ZnO thin films. The sharp edge at 150 nm for sample 2 is due to the absorption of glass substrate. The several broad bands below 360 nm (3.3 eV) are due to the band-to-band transition of ZnO. The sample 2 is efficiently transparent as TCO thin film above 380 nm (visible light region), while the sample 1 is not so.

Figure 2 shows the luminescence spectra with various excitation wavelengths in sample 2 at 300 K. The band-to-band excitation below 360 nm produces two broad luminescence bands. In these spectra, the additional peaks around 540 and 590 nm are the influence from outer lights, which could not be perfectly eliminated. As the excitation wavelength increases (the energy decreases), the intensity of luminescence band around 570 nm decreases, while that around 420 nm still remains.

Figure 3 shows the luminescence spectra in sample 2 at 10 K. The spectrum with the 100 nm excitation shows no dent around 480 nm, in other words, both bands around 420 nm and 570 nm get broader and closer. With increasing the excitation wavelength, the luminescence intensities decrease. As a consequence, the band around 420 nm remains, whereas that around 570 nm almost disappears.

The band around 420 nm is estimated to be intrinsic luminescence (for example, self-trapped exciton). The broader band around 570 nm is estimated to be the luminescence associated with defects (for example, donor/acceptor recombination).

The relation between the luminescence and electrical conductivity will be examined. In this study, optical properties of pure ZnO thin films were investigated. It seems to be more important to investigate Ga or Al doped ZnO thin films in the point of electrical conductivity.

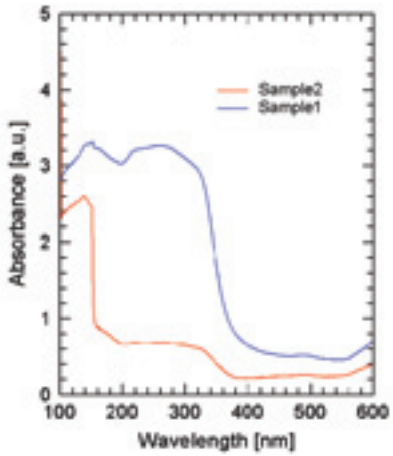


Fig. 1. Absorption spectra in ZnO thin films at 300 K.

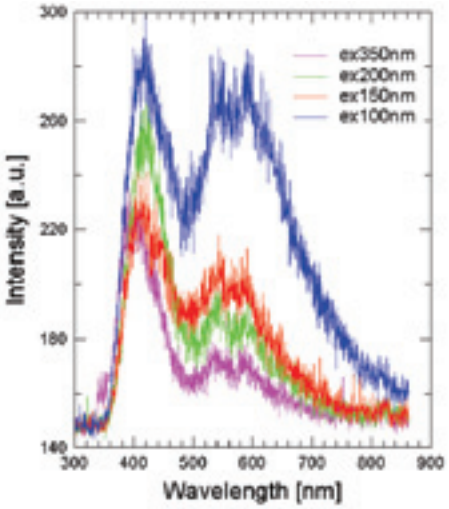


Fig. 2. Luminescence spectra in sample 2 at 300 K.

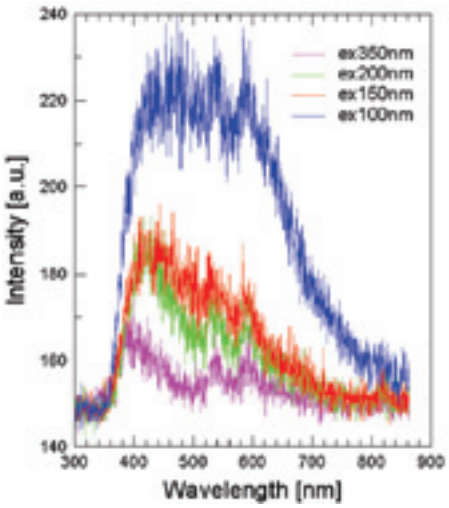


Fig. 3. Luminescence spectra in sample 2 at 10 K.

BL1B

# Optical Spectroscopy of Wide Gap Semiconductors

M. Yamaga, H. Uno, Y. Ogoshi, A. Kanetake, S. Takano and T. Nohisa
*Department of Material and Design Engineering, Gifu University, Gifu 501-1193, Japan*

$In_xGa_{1-x}N$ and $Cd_{1-x}Mn_xTe$ crystals are wide band-gap semiconductors. Band-gap energies of indium gallium nitride ($In_xGa_{1-x}N$) mixed crystals decrease with increasing $x$. Absorption edges of $In_xGa_{1-x}N$, corresponding to the band-gap energies, vary from the ultraviolet to visible ranges. Then, $In_xGa_{1-x}N$ mixed crystals are a promising material for multi-junction thin film solar cells. On the other hand, $Cd_{1-x}Mn_xTe$ crystals have magneto-optical properties induced by $Mn^{2+}$ ions. They are useful as an optical isolator material.

$In_xGa_{1-x}N$ thin films were deposited on $SiO_2$ substrates by rf-sputtering at room temperature. Sputtering targets were In and Ga metals with various weight ratios. The X-ray diffraction (XRD) patterns of the $In_xGa_{1-x}N$ thin films consisting of several peaks in the angle range between 30 and 70 degrees indicate microcrystalline thin films.

$Cd_{1-x}Mn_xTe$ single crystals were grown by the vertical Bridgeman method. The composition of the crystal is the same as the melting composition.

Figure 1 shows absorption spectra observed in $In_{0.2}Ga_{0.8}N$ and $Cd_{0.5}Mn_{0.5}Te$ at 300 K. The absorption edge of the GaN thin film was observed at 360 nm at room temperature, whereas that of $In_{0.2}Ga_{0.8}N$ thin film is shifted toward a longer wavelength of about 450 nm as shown in Fig.1. The absorption spectrum of $Cd_{0.5}Mn_{0.5}Te$ consists of several broad bands in the range from 100 to 600 nm.

It is reported that GaN crystals show sharp exciton luminescence around 360 nm and substitution of In in GaN crystals leads to red-shift and line-broadening of the luminescence. UV excitation for the $In_{0.2}Ga_{0.8}N$ thin film produces broadband luminescence with double peaks at 460 and 560 nm as shown in Fig. 2. The luminescence for the GaN thin film is similar to that for $In_{0.2}Ga_{0.8}N$ thin film. This result suggests that the 460 and 560 nm luminescence broadbands may be associated with N deficits and impurity O ions.

Figure 3 shows temperature dependence of the luminescence spectra excited at 100 nm for $Cd_{0.5}Mn_{0.5}Te$. The peak energy of the luminescence is just below the band edge energy in Fig. 1. The luminescence intensities markedly decrease above 120 K. The luminescence may be due to weakly localized excitons.

Identification of these luminescence centers $In_xGa_{1-x}N$ and $Cd_{1-x}Mn_xTe$ crystals gives information on structure and energy levels of the localized luminescence centers.

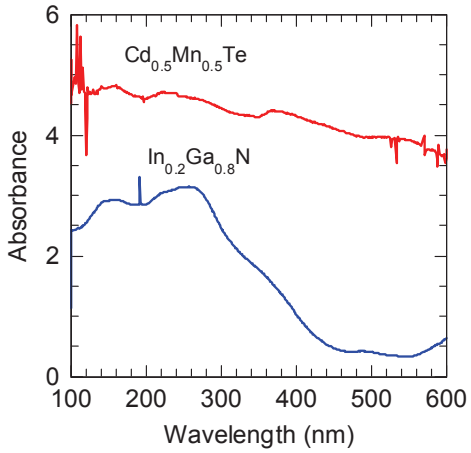


Fig. 1. Optical absorption spectra at 300 K.

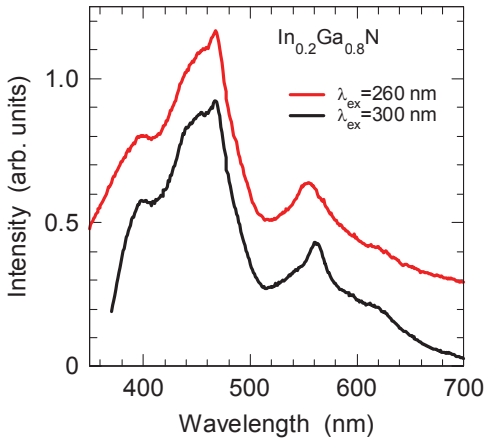


Fig. 2. Luminescence spectra in $In_{0.2}Ga_{0.8}N$.

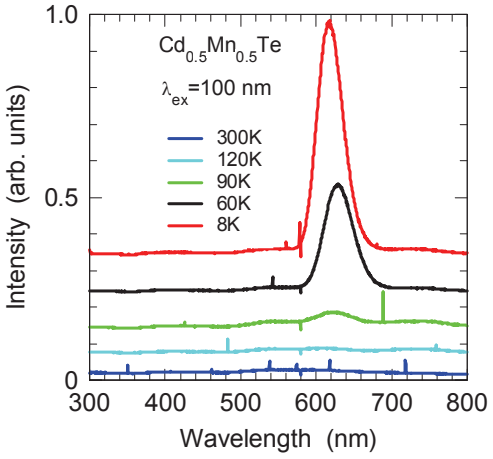


Fig. 3. Luminescence spectra in $Cd_{1-x}Mn_xTe$.

BL3U

# Soft X-Ray Emission Spectroscopy in the C $K_\alpha$ of Graphene-Nanoflakes (GNFs) Functionalized with Nitrogen

J. W. Chiou[1], M. T. Liou[2], W. F. Pong[2], H. Yamane[3] and N. Kosugi[3]
[1] *Department of Applied Physics, National University of Kaohsiung, Kaohsiung, Taiwan*
[2] *Department of Physics, Tamkang University, Tamsui, Taiwan*
[3] *Institute for Molecular Science, Okazaki 444-8585, Japan*

Figure 1 shows normal x-ray emission spectra (NXES) and Figure 2 shows resonant inelastic x-ray scattering (RIXS) spectra excited at different photon energies in the spectra of the C $K_\alpha$ of HOPG and GNFs:N deposited on Si(100) substrate, prepared using microwave plasma enhanced chemical vapor deposition process and subsequently functionalized with nitrogen plasma by the electron cyclotron resonance process. Spectral features of these GNFs:N films are essentially similar, consisting of a broad main feature around 277.4 eV (A) and a high-energy shoulder feature near 281.7 eV (B), to those observed by Muramatsu *et al*. [1]. However, the peak-to-height ratio of the shoulder-feature to the main-feature depended on the nitrogen at.% (0 to 20 at.%). These spectral features therefore suggest that local electronic structures and chemical bonding states are essentially similar among the GNFs:N films, but that their ratios, for example of $sp^2$ and $sp^3$-configured carbon atoms, differ depending on the nitrogen at. %. Comparing the spectra of GNFs films and reference HOPG, we conclude that the main feature (A) is in same position with HOPG and the high-energy shoulder feature (B) of the GNFs films are not in the same position as slightly shifts towards higher energy than in HOPG. These features A and B are the σ and π orbitals, respectively. The feature height and their ratios are tabulated in Table 1. It is very difficult to draw some conclusion on the (π/σ) ratio presently because on nitrogen functionalization initially it decreases and then increases indicating the change of $sp^2/sp^3$ ratio.

Figure 2 shows that the spectral features are varied with the excitation energy, indicating $sp^2$ and/or $sp^3$ carbons are resonantly excited at certain excitation of energy. The redistribution of intensities in the spectra indicates changes in the occupancies of different molecular orbitals, possibly due to changes in electron density of states upon nitrogen incorporation in GNFs:N. The NXES spectral profile has been used as a means to identify certain chemical states of incorporation of nitrogen in the GNFs structure. However, it is also observed in Fig. 2 that the C $K_\alpha$ RIXS spectra strongly depend on excitation energy and the dependence is believed to stem from the resonant inelastic scattering and related to the band structure of the GNFs:N. This interpretation is important for all the emission experiments with high resolution synchrotron radiation and implies the possible use of photon-in-photon-out technique for electronic band structures. This soft NXES/RIXS revealed a new picture of the core excitation and the existence of strong vibronic coupling effects in GNFs and GNFs:N.

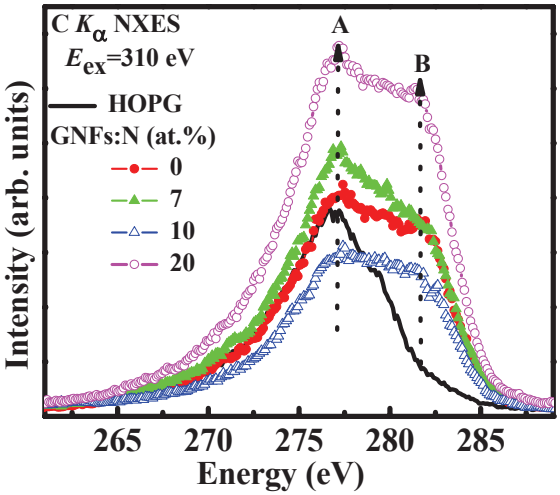


Fig. 1. NXES spectra of HOPG and GNFs:N.

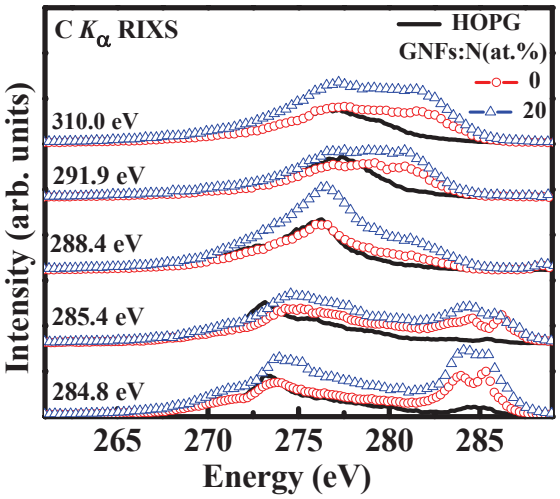


Fig. 2. RIXS spectra of HOPG and GNFs:N.

Table 1. Intensity of σ and π and their ratios.

| | Peak B (π) | Peak A (σ) | (π/σ) ratio |
|---|---|---|---|
| HOPG | 26.3 | 37.5 | 0.70 |
| GNFs | 36.2 | 41.2 | 0.88 |
| GNFs:N(7at.%) | 34.3 | 47.7 | 0.72 |
| GNFs:N(10at.%) | 26.2 | 31.2 | 0.84 |
| GNFs:N(20at.%) | 58.2 | 66.4 | 0.88 |

[1] Y. Muramatsu *et al*., Carbon **39** (2001) 1403.

BL3U

# Probing Electronic Structure of Graphdiyne by Resonant Soft-X-Ray Emission Spectroscopy

J. Zhong[1], T. Xie[1], X. H. Sun[1], S. D. Wang[1], Y. L. Li[2], H. Yamane[3], N. Kosugi[3] and J. H. Guo[4]

[1]*Jiangsu Key Laboratory for Carbon-Based Functional Materials and Devices, Institute of Functional Nano and Soft Materials Laboratory (FUNSOM), Soochow University, Suzhou 215123, China*

[2]*Institute of Chemistry, Chinese Academy of Sciences, Beijing 100190, China*

[3]*Institute for Molecular Science, Okazaki 444-8585, Japan*

[4]*Advanced Light Source, Lawrence Berkeley National Laboratory, Berkeley, CA 94720, USA*

The structural study of carbon is a main fundamental interest and is expected to be widely applied to nanosciences and technology. Due to carbon's three hybridization states ($sp^3$, $sp^2$ , and sp), having numerous combinations by which atoms of this element can be bonded to each other to produce many carbon allotropes; such as graphite ($sp^2$), diamond ($sp^3$) in the nature, and many novel carbon allotropes such as fullerene ($sp^2$), carbon nanotube ($sp^2$), and graphene ($sp^2$), are successfully synthesized. The design and synthesis of new carbon allotropes with definite structure and property is a significant and ongoing challenge within new materials science and there are still a large number of new forms of carbon to be discovered. Graphdiyne proposed is a novel structure in the carbon family and predicted to be the most stable of the various diacetylenic nonnatural carbon allotropes and is one of the most "synthetically approachable" [1]. Recently, the synthesizing of a novel, stable graphdiyne form of carbon has been reported and in this work, we probe the electronic structure of graphdiyne in comparison with that of highly oriented pyrolitic graphite (HOPG), single-walled carbon nanotube (SWNT) and graphene by using resonant soft-x-ray emission spectroscopy (XES).

X-ray absorption spectroscopy (XAS) probes the unoccupied density of states (DOS) and XES probes the occupied DOS. In addition to the inherent elemental selectivity of X-ray spectra, energy selective excitation of the emission spectra allows separation of features that pertain to different atoms or same element in different chemical environments. In previous report [2], the quantum confinement of SWNT with decreased tube diameters has been reported which can be observed in resonant emission spectra by significant changes in the π and σ bands. Figure 1 shows the C *K*-edge resonant emission spectra of HOPG, SWNT, graphene and graphdiyne at the excitation energy of 285.5 eV. The spectrum for graphdiyne in the σ band shows great changes compared to that for HOPG and SWNT, while similar to that for graphene, indicating a similar hybridization as graphene. Figure 2 shows the C *K*-edge normal emission spectra at the excitation energy of 305 eV. A difference in the σ band for graphdiyne can be found compared to all other samples, indicating the specific electronic structure of graphdiyne.

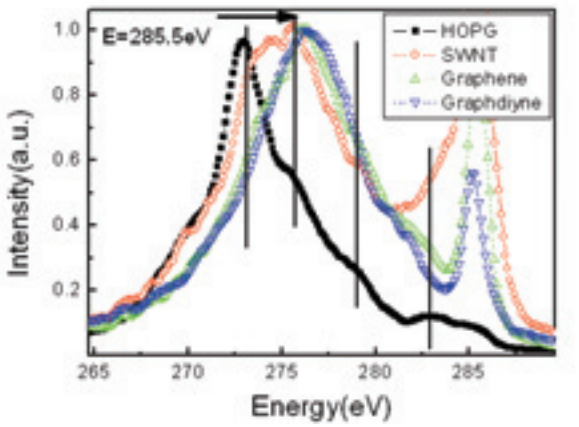


Fig. 1. C *K*-edge resonant emission spectra of HOPG, SWNT, graphene and graphdiyne at the excitation energy of 285.5 eV.

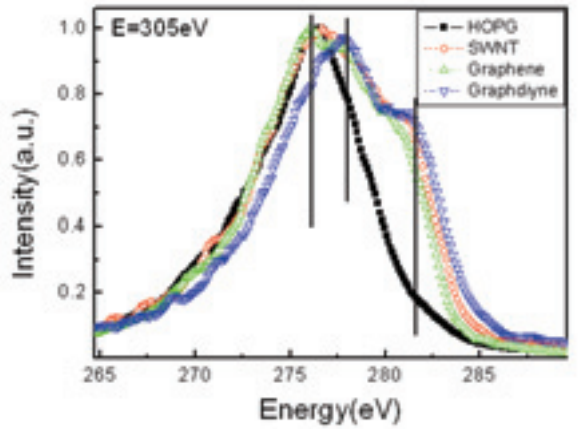


Fig. 2. C *K*-edge normal emission spectra of HOPG, SWNT, graphene and graphdiyne at the excitation energy of 305 eV.

[1] G. X. Li, Y. L. Li, H. B. Liu, Y. B. Guo, Y. J. Li and D. B. Zhu, Chem. Comm. **46** (2010) 3256.
[2] J. Zhong *et al.*, Appl. Phys. Lett. **93** (2008) 023107.

BL4B

# Synchrotron Radiation Effect on the Local Structure of Highly-Hydrogenated Diamond-Like Carbon Film

K. Kanda, M. Uemura and T. Hasegawa
*Laboratory of Advanced Science and Technology for Industry, University of Hyogo, Ako 678-1205, Japan*

Diamond-like carbon (DLC) film is expected to use as lubrication material in space, where oil cannot be used, because its some excellent properties such as hard, low friction coefficient, low surface energy and so on. It was known that the DLC films are durable against X-ray exposure, because it was reported that DLC films are not etched by exposure to soft X-ray (SX) in the absence of oxygen gas [1]. However, many kinds of novel DLC films have been fabricated by the remarkable advancement in DLC industry in last decade. Recently, irradiation of SX in a vacuum into DLC films has been reported to lead the desorption of hydrogen and an increase in the film density, hardness, and refractive index [2]. Information on the mechanism of the deterioration of DLC film by X-ray exposure is undoubtedly important for use of DLC films in space safely.

In the previous study [3], we reported that the SX exposure in the vacuum with the absence of oxygen to the DLC films formed using the amplitude-modulated RF CVD method leaded to the desorption of hydrogen and etching. In the present study, we measured NEXAFS spectra of the DLC films at BL8B1 of UVSOR to discuss of the variation of local structure of DLC film by the irradiation of SX.

DLC films were deposited with 200-nm thickness on Si wafers by using the amplitude-modulated RF plasma-enhanced CVD method. Three kinds of DLC film, each with different hydrogen content, were used as samples. The SX irradiation of the DLC film was carried out at beamline 6 (BL-6) of NewSUBARU synchrotron facility in the University of Hyogo. The electron energy of the NewSUBARU ring was 1.0 GeV and the ring current was 220 mA on a top-up mode. The synchrotron radiation (SR) at the BL-6 sample stage had a continuous spectrum from IR to soft X-rays, which are lower than 1 keV. Sample DLC films were exposured to SR at room temperature.

Local structure was evaluated from the Near edge X-ray absorption fine structure (NEXAFS) study performed at the BL4B of UVSOR. The NEXAFS spectra were measured in the energy range 275-320 eV with 0.5 eV FWHM resolution in the total electron yield mode.

A pre-edge resonance at 285.4 eV is not visible in the spectrum of diamond because diamond consists of only carbon atoms in $sp^3$ (C-C) sites. Therefore, the peak intensity of this resonance is considered as a good index of $sp^2$ content. The procedure for determination of $sp^2$ content from the NEXAFS measurements was established in the previous studies [4, 5]. The amount of $sp^2$ bonded carbon atoms can be extracted by normalizing the area of the resonance corresponding to 1s→π* transitions at 285.4 eV with the area of a large section of the spectrum. The absolute $sp^2/(sp^2+sp^3)$ ratio was determined by the comparison with that from the NEXAFS spectrum of graphite.

The $sp^2/(sp^2+sp^3)$ ratio in the DLC film, estimated from NEXAFS study, was plotted to irradiated SR dose in Fig.1. The $sp^2/(sp^2+sp^3)$ ratio increased steeply from ≈0.5 before irradiation of SR to ≈0.6 after the irradiation of SR of 300 mA·h dose. Beyond 300 mA·h dose, the $sp^2/(sp^2+sp^3)$ ratio keeps ≈0.6. As a result, carbon double bonding can be regarded to formed due to the desorption of hydrogen from highly-hydrogenated DLC film in the dose region under 300 mA·h.

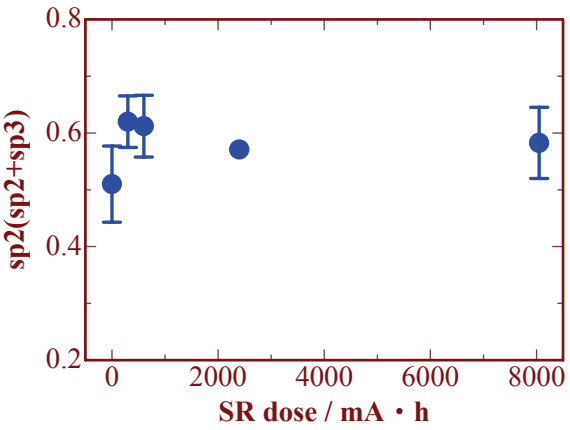


Fig. 1. Dose dependence of $sp^2/(sp^2+sp^3)$ ratio in the DLC film

[1] H. Kyuragi and T. Urisu, Appl. Phys. Lett. **50** (1987) 1254.
[2] H. Matsuura, S. Ohkubo, K. Oda and T. Ushiro, SEI Technical Review **171** (2007) 39 (Japanese).
[3] K. Kanda, K. Yokota, M. Tagawa, M. Tode, Y. Teraoka and S. Matsui, Jpn. J. Appl. Phys. to be published.
[4] K. Kanda, T. Kitagawa, Y. Shimizugawa, Y. Haruyama, S. Matsui, M. Terasawa, H. Tsubakino, I. Yamada, T. Gejo and M. Kamada, Jpn. J. Appl. Phys. **41** (2002) 4295.
[5] K. Kanda, Y. Shimizugawa, Y. Haruyama, I. Yamda, S. Matsui, T. Kitagawa, H. Tsubakino and T. Gejo, Nucl. Instrum. Methods Phys. Res. B **206** (2003) 880.

BL4B, BL1A

# Study on the Electronic Structures of the Layered $Li_2MO_3$-$LiMO_2$ Materials in Li De-Intercalation Process

H. Kobayashi[1] Y. Takenaka[2] and M. Shikano[1]

[1]*Research Institute for Ubiquitous Energy Devices, AIST, Ikeda, Osaka 563-8577, Japan*

[2]*Department of Chemistry and Materials Engineering, Faculty of Chemistry, Materials and Bioengineering, Kansai University, Suita, Osaka 564-8680, Japan*

The layered $Li_2MO_3$-$LiMO_2$ ($M$ =transition metal) materials are one of the promising positive electrode materials of lithium secondary battery because of their large capacity when operated above 4.6 V [1]. Especially, $Li[Ni_{0.17}Li_{0.2}Co_{0.07}Mn_{0.56}]O_2$ displays a 1st discharge capacity of c.a. 280 mAh/g in the voltage range of 2.5 to 4.8 V and keep a reversible capacity of c.a. 250 mAh/g after 50 cycles [2]. Several papers have reported on the mechanism why these materials show large reversible capacity. However, the initial charge and discharge process are still ambiguous. We have reported on the characteristic structural change during Li de-intercalation for $LiNi_{1/2}Mn_{1/2}O_2$ [3,4] using synchrotron radiation. Detailed information on the crystal and electronic structures above 4.6 V is very important in order to improve the calendar life and thermal stability of these materials and, therefore, the structural changes of $Li_{1.01}Ni_{0.49}Co_{0.21}Mn_{0.29}O_2$ (Sample A) and $Li_{1.20}Ni_{0.17}Co_{0.10}Mn_{0.53}O_2$ (Sample B) were investigated in Li de-intercalation process.

The de-lithiated samples from samples A and B were electrochemically prepared using coin-type cells with Li/1M $LiPF_6$ in EC:DMC(1:2)/samples. Electronic structures were investigated by the total electron yield mode at BL4B and BL1A in UVSOR. The data were analyzed using the program Athena.

Figure 1 shows the 1st charge curves of the samples A and B in the voltage range of 2.0 and 4.8 V. The Li/Sample A cell showed the 1st charge capacity of 282 mAh/g with the characteristic plateau region around 4.5 V. On the other hands, the Li/Sample B cell showed the 1st charge capacity of 251 mAh/g without plateau region.

Figure 2 shows the Ni L-edge XANES spectra for the de-lithiated samples from the samples A and B (BL4B). The spectrum measured contained peaks a and b, corresponding to the valence state of 2+ and 3~4+, respectively. The sample A showed that the intensity of peak b increased to y=0.8 with Li de-intercalation. On the other hand, the sample B showed that the maximum of peak b was observed at y=0.4. These results indicate that Li de-intercalation mechanism is different between these samples.

[1] A. Ito *et al.*, J. Power Sources **183** (2008) 344.
[2] A. Ito *et al.*, J. Power Sources **195** (2010) 567.
[3] Y. Arachi *et al.*, Solid State Ionics **176** (2005) 895.
[4] H. Kobayashi *et al.*, J. Power Sources **146** (2005) 640.

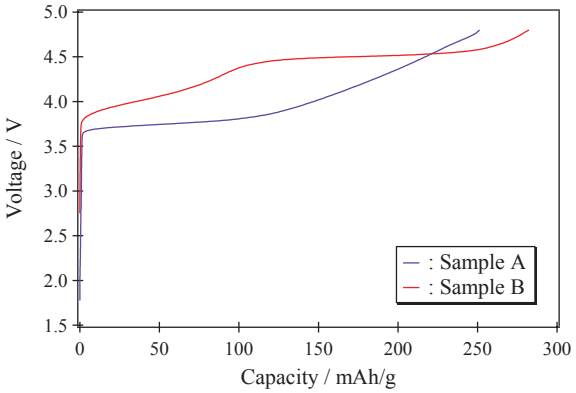


Fig. 1. 1st charge curves for the samples A and B.

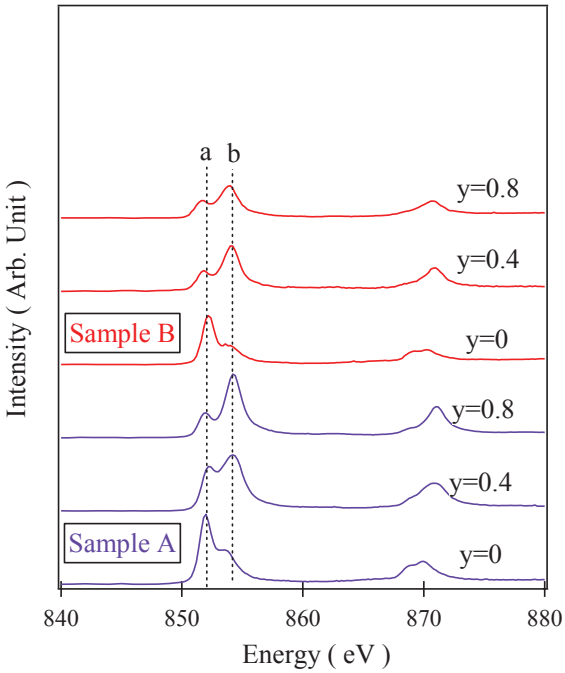


Fig. 2. Ni L-edge XANES spectra for the de-lithiated samples from the samples A and B (BL4B).

BL5U

# Effects of Periodicity Imperfection on Mini-Bands in Semiconductor Superlattice

K. Hashimoto[1], T. Ujihara[1], Y. Maeda[1], M. Kuwahara[2], H. Miyazaki[3] and Y. Takeda[1]
[1]*Graduate School of Engineering, Nagoya University, Nagoya 464-8603, Japan*
[2]*EcoTopia Science Institute, Nagoya University, Nagoya 464-8603, Japan*
[3]*UVSOR Facility, Institute for Molecular Science, Okazaki 444-8585, Japan*

Recently, a quantum dot solar cell is proposed to achieve a high conversion efficiency that can reach over 50%, theoretically. The concept of the quantum dot solar cell is to utilize mini-bands in the periodic alignment of quantum dots as a middle band in the carrier excitation in order that the band structure is adjusted to the solar light spectrum. The theoretical calculation is based on an assumption of "the perfectly periodic potential." However, it is presently impossible to produce quantum dots of equal size and perfect periodicity. In this study, the effects of periodicity imperfection on the mini-band structure, especially hole mini-bands, were investigated. In place of aligned quantum dots, we examined a superlattice structure which consists of multiple quantum wells because the preparation method has been established.

We fabricated three specimens: a GaAs bulk sample, an AlGaAs/GaAs superlattice, and a disordered AlGaAs/GaAs superlattice. Figure 1 shows the detailed structures of each sample. The second well layer in the disordered superlattice was made thicker. Amorphous arsenic layers were deposited on the sample surfaces to suppress oxidation. The arsenic layer was thermally removed just before measurements. On the evaluation of the mini-band structure, the synchrotron-radiation photoemission measurements at BL5U of the UVSOR facility were performed.

Figure 2 shows the energy spectra in a valence band around Γ point. These mappings were processed by the second order differential with respect to the binding energy. There are mainly two bands that are symmetrical at the red arrows. The lower and higher energy bands are thought to be a heavy hole band and a light hole band, respectively. Theoretically, heavy hole band and light hole band in GaAs are doubly-degenerated at the Γ point. But, in the present result, these bands are split and its width of the GaAs sample is 180 meV corresponding to the width of band splitting at the wavenumber $k_{//}$ = 0.0669 Å$^{-1}$. Thus, these mappings show the band structures at this wavenumber.

The bands of (a) GaAs and (b) periodic superlattice are widely dispersive, while those of (c) disordered superlattice are flatter. The width of dispersion depends on the degree of confinement effect. This flatter band is considered to be due to the quantum level in the thicker well layer.

Figure 3 shows widths of band splitting between the heavy hole band and the light hole band as a function of wavenumber. We found that the band splitting width of superlattice is larger than that of GaAs bulk. As far as we know, this result is the first direct observation of the band splitting due to the mini-bands of the ordered superlattice. The splitting energy of the disordered superlattice is wider comparing to that of GaAs. However, the wavenumber dependence is small because the band splitting is due to the narrow quantum level in the quantum well. These results imply that a disorder of only one layer in superlattice disturbs the ideal mini-band structure.

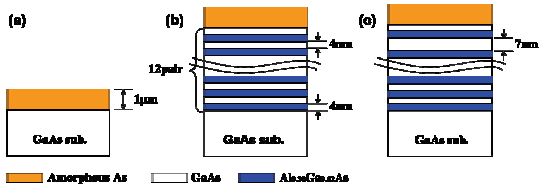


Fig. 1. Schematic images of the sample structure. (a) GaAs bulk sample, (b) periodic superlattice and (c) disordered superlattice.

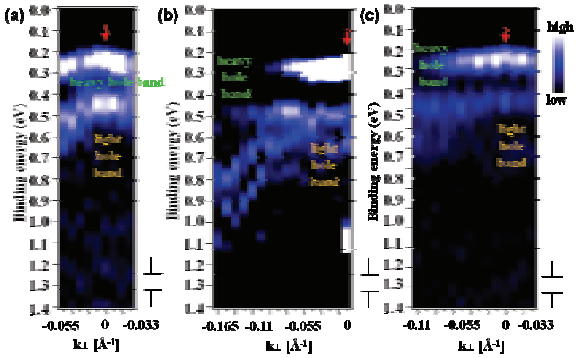


Fig. 2. Photoemmision spectra of (a) GaAs bulk sample, (b) periodic superlattice and (c) disordered superlattice.

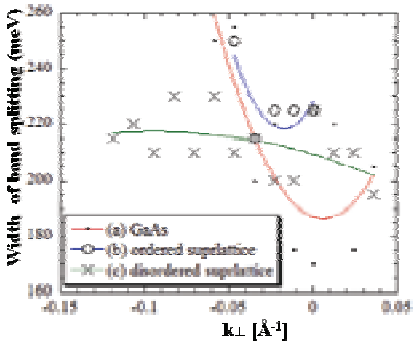


Fig. 3. Width of band splitting between heavy hole band and light hole band.

BL5U

# Angle-Resolved Photoemission Study on Epitaxial Graphene Grown on SiC(0001)

A. Ruammaitree, H. Hu, H. Nakahara, K. Akimoto, S. Harada, K. Soda and Y. Saito
*Department of Quantum Engineering, Graduate School of Engineering, Nagoya University, Nagoya 464-8603, Japan*

Graphene, which has many exotic properties such as high mobility and linear dispersion (Dirac cone) at the K-point in the Brillouin zone, can be synthesized by various methods. Annealing SiC is one of the efficient approaches for a large scale production of graphene [1], where it is important to control the layer number of grown graphene. To determine its layer number, there are several techniques such as Auger electron spectroscopy, x-ray photoelectron spectroscopy and ellipsometry. The accuracy of their techniques depends on their models. In this report, not only the electronic structure but also the estimation of layer number of graphene epitaxially grown on SiC is studied by angle-resolved photoemission spectroscopy (ARPES). The result can give us the accurate number of the epitaxial graphene layers.

The epitaxial graphene on an n-type Si-terminated 6H-SiC(0001) substrate of 12×3×0.25 $mm^3$ (CRYSTAL BASE co. ltd.) was prepared by annealing it in an atmosphere of argon, as follows. After ultrasonic cleaning with acetone, the substrate was immediately mounted on a sample holder and put in a chamber with the base pressure of ~$10^{-8}$ Pa. In order to remove oxides on the substrate surface, we deposited silicon around 2 monolayers on it. Si molecules deposited are expected to crash and eliminate the oxide molecules from the surface. Then the sample was transferred, without exposure to air, to an argon chamber where it was annealed by resistive heating in the atmosphere of argon. The annealing temperature was measured by an optical pyrometer. The epitaxial growth of graphene was confirmed by reflection high energy electron diffraction (RHEED). The transverse and longitudinal orientations of the substrate are [-1, 0, 1, 0] and [-1, 2, -1, 0], respectively, and the unit cell of the graphene rotates by 30 degrees to the SiC cell.

The ARPES measurement was conducted at room temperature with a hemispherical electron analyzer (MBS A-1) and a circularly polarized photon beam as an excitation source. To obtain a clear Dirac cone image at the K point, the excitation photon energy was set to 80 eV and the angle between the photon beam and the surface normal was 23 degrees. Total energy resolution including the thermal broadening was estimated to be 0.12 eV by measuring the Fermi edge of an Au film.

ARPES is one way for estimating the layer number of epitaxial graphene [2]**.** Figure 1 shows the electronic structure around the K point (zero wave number in the figure) for the sample prepared by annealing at 1948 K under the argon pressure of 0.03 MPa. The green dot curves represent π and π* bands which originate from double layered graphene, while the red lines stand for a linear dispersion of a graphene monolayer. The presence of a brighter curve in the valence band and a bright area in the band gap suggests that this sample may be composed of the monolayer and bilayer graphenes. This is consistent with our x-ray diffraction observation of the averaged layer number of ~1.6, which will be reported elsewhere.

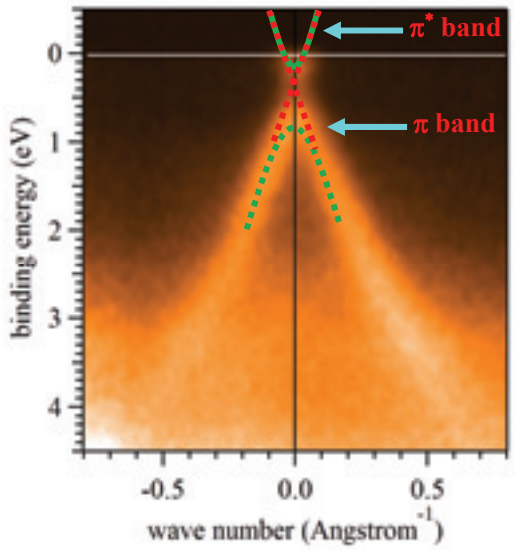


Fig. 1. Electronic band dispersion around the K point (zero wave number) of the graphene of the SiC(0001), which was synthesized by annealing at 1948 K under the argon pressure of 0.03 MPa.

[1] J. Hass *et al*., J. Phys.: Condens. Matter **20** (2008) 323202.
[2] T. Ohta *et al*., Phys. Rev. Lett. **98** (2007) 206802.

BL5U

# Valence-Band Structure of $Mg_2Si$ in High-Pressure Phase

K. Soda, T. Shimada, H. Kondo, S. Harada, K. Nishida and M. Hasegawa
*Graduate School of Engineering, Nagoya University, Nagoya 464-8603, Japan*

Valence-band electronic structure has been studied for $Mg_2Si$ in a metastable hexagonal high pressure phase by photoelectron spectroscopy. Semiconducting $Mg_2Si$ and its related compounds have received much attention because of its high thermoelectric properties with light constituent elements [1-3]. $Mg_2Si$ in a normal pressure phase show n-type thermoelectric power, probably due to Mg-derived defects, and its related p-type compounds are desired to develop. Recently we have found high p-type thermoelectric power and large electric conductivity for the metastable high pressure phase. According to a band structure calculation [3], the fundamental band gap is expected to collapse to a pseudogap in so far reported high pressure phases, orthorhombic anti-cotunnite (> 7.5 GPa at room temperature) and hexagonal $Ni_2In$-type (> 21.3 GPa) structures. However, the electronic structure has not been clarified for the present high pressure phase yet.

Specimens of metastable hexagonal high pressure phase $Mg_2Si$ were prepared under 7 GPa at 1173 K by multi-anvil cell. $Mg_2Si$ in a normal pressure phase was also obtained by pressing $Mg_2Si$ powder without annealing. Valence-band spectra were recorded at 10 K with a total energy resolution of 0.12 eV at the excitation photon energy $h\nu$ of 70 eV. The origin of the binding energy $E_B$ was set to the Fermi energy $E_F$ of a reference Au film electrically connected to the specimen. Although the specimens were *in situ* fractured or filed to clean their surfaces for the photoelectron measurement, contamination by oxide species, unfortunately, was not completely removed. However, it seems not to affect the valence-band structure near $E_F$ so much, since the bands of the oxide species are located at $E_B > \sim 4$ eV [6, 7].

Figure 1 shows typical valence-band spectra near $E_F$ of $Mg_2Si$ in the normal and high pressure phases together with an Au spectrum and density of states (DOS) for the normal pressure phase, which was calculated by an all-electron full-potential linearized augmented plane wave (FLAPW) method with the WIEN2k code [4] at the experimental lattice constant $a$ = 0.6354 nm of the anti-fluorite structure. Calculated indirect band gap of ~ 0.2 eV is narrower than experimentally reported (0.63 eV [3] and 0.77 eV [5]), which may be partly attributed to the well-known tendency in the density functional calculation. The spectral intensity is normalized at $E_B$ ~ 2 eV and the origin of $E_B$ for the calculated DOS is set to the conduction bottom because of the n-type thermoelectric properties of the normal pressure phase. For the normal pressure phase, the spectral intensity decreases towards $E_F$, as predicted. However, a small but definite intensity is observed around $E_F$, which might be ascribed to defect states within the band gap and might even imply the conduction bottom near $E_F$ as expected by the band structure calculation and the n-type thermoelectric power. On the other hand, the intensity at $E_F$ is clearly increased and the valence band top moves to $E_F$ for the high pressure phase. This is consistent with both the high electric conductivity and the p-type thermoelectric power, although it is difficult to study the unoccupied conduction band by photoelectron spectroscopy.

Further study is intended for specimens synthesized in Ar atmosphere.

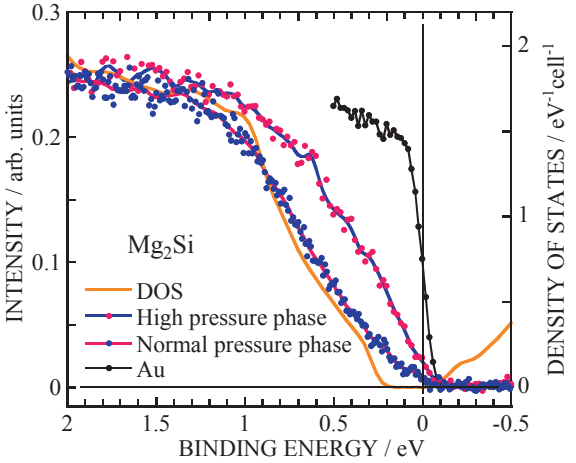


Fig. 1. Valence-band photoelectron spectra of $Mg_2Si$ in normal and high pressure phases. Fermi edge of a reference Au film and calculated density of states (DOS) of normal pressure phase $Mg_2Si$ are also shown for comparison.

[1] Y. Noda *et al.*, J. Jpn. Inst. Mtals **53** (1989) 487.
[2] M. Akasawa *et al.*, J. Appl. Phys. **104** (2008) 013703.
[3] F. Yu *et al.*, Solid State Commun. **150** (2010) 620.
[4] K. Schwarz *et al.*, Comp. Phys. Commun. **147** (2002) 71.
[5] U. Winler, Helv. Phys. Acta. **28** (1955) 633.
[6] M. Cardona *et al.*, Phys. Stat. Sol. **58** (1973) 483.
[7] M. Brause *et al.*, Surf. Sci. **398** (1998) 184.

BL5B

# In-situ Observations of Photoinduced Effects on Amorphous Chalcogenide Semiconductors by Synchrotron Orbital Radiation

K. Hayashi

*Department of Electrical and Electronic Engineering, Gifu University, Gifu 501-1193, Japan*

## Introduction

It is well known that amorphous chalcogenide semiconductor materials show a variety of photoinduced effects [1-3]. Photodarkening (photoinduced optical absorption edge shift), photodegradation (photoinduced defect creation) and photoinduced volume change are representative photoinduced phenomena. These phenomena are caused by irradiation of light (bandgap (BG) light) having photon energy comparable to the optical bandgap. These phenomena can in general be either irreversible, i.e. the photoinduced changes are permanent after irradiation, or reversible, in which case the changes can be removed by annealing to the glass-transition temperature. The photoinduced changes by BG light of the x-ray diffraction and the volume have directly shown that these phenomena are due to a change of the local structure of the amorphous network. Several previous studies of photoinduced effects have reported that there is no direct correlation among photodegradation, photodarkening and photoinduced volume change. The detail is not clarified though the dynamics of those photoinduced effects certainly seems to be different.

Our recent studies have focused on the photoinduced energy structure changes in the vacuum ultraviolet (VUV) region by irradiation of BG light. To obtain a wide knowledge of the photoinduced phenomena, we have investigated photoinduced effects in the VUV region by the transmission spectra of amorphous thin films prepared onto polymer membrane substrates. In previous work, we reported the VUV transmission spectra of substrate-free evaporated amorphous thin films that removed the substrate [4]. Few studies have examined whether the photoinduced change of the chemical bonds contributes to photodarkening and photodegradation. To understand the dynamics and the correlation of photoinduced structure changes in the VUV region and the photodegradation in amorphous chalcogenide semiconductors, real time in-situ measurements are required. However, it is difficult to measure the transmission change while irradiating the BG light. Therefore, those dynamics and correlations are examined by measuring the total photoelectron yield (TPEY) that can measure the optical property in the VUV region. In this report, we will compare the transmission spectrum and the TPEY spectrum in the amorphous thin films.

## Experimental

Samples used for the measurement of the transmission spectrum were substrate-free evaporated amorphous chalcogenide (a-$As_2S_3$ and a-$As_2Se_3$) semiconductor thin films. Samples used for the measurement of the TPEY spectrum were prepared onto quartz substrates which fabricated gold electrodes by conventional evaporation technique. The thickness of the amorphous films was from around 160 nm to 300 nm. The measurements were performed at room temperature at the BL5B beam line. A pinhole of 1.5 mm in a diameter was inserted between the monochromator and sample to remove stray light. The intensity of the VUV light was monitored by measuring the TPEY of a gold mesh.

## Results and Discussion

Figure 1 shows the VUV transmission spectrum and the TPEY spectrum of a-$As_2S_3$ films at room temperature. It is necessary to note it because the intensity correction by incident light strength is not performed as for both spectra. As shown in the figure, the absorption peak corresponds very well in both spectra. The escape depth of the photoelectrons and the creation of the secondary electrons might influence the difference of both spectral line shapes. It will be necessary to discuss this point in the future.

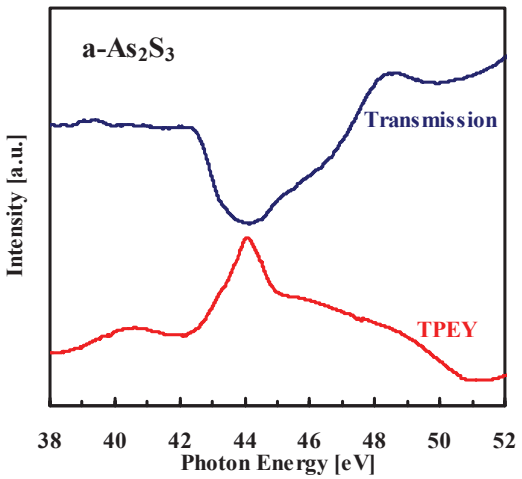


Fig. 1. VUV transmission and total photoelectron yield (TPEY) spectra of a-$As_2S_3$ film.

[1] Ke. Tanaka, Rev. Solid State Sci. **4** (1990) 641.
[2] D. L. Staebler and C.R. Wronski, Appl. Phys. Lett. **31** (1977) 292.
[3] S. R. Elliot, J. Non-Cryst. Sol. **81** (1986) 71.
[4] K. Hayashi, UVSOR Activity Report **34** (2006) 79.

BL5B

# Characterization of 10-Bilayer $TiO_2$/ZnO Mirrors at 2.74 nm

H. Kumagai[1], Y. Tanaka[1], M. Murata[1], M. Sanjo[1], T. Shinagawa[2] and M. Chigane[2]
[1]*Graduate School of Engineering, Osaka City University, Osaka 558-8585, Japan*
[2]*Inorganic Materials Lab., Osaka Municipal Technical Research Institute, Osaka 536-8553, Japan*

The authors have proposed the use of a novel metal oxide multilayer for soft-x-ray reflectors at water-window wavelengths [1], because an oxide multilayer can prevent the formation of an alloy at the interface without any buffer layer, and the absorption of oxygen in oxides is negligible at water-window wavelengths; moreover, the metal oxide multilayer can be fabricated by atomic layer deposition or atomic layer epitaxy (ALE). These techniques can be used to control surfaces on an atomic scale by sequentially dosing the surface with appropriate chemical precursors and then promoting surface chemical reactions that are inherently self-limiting. We have found that the self-limiting adsorption mechanism is effective in the fabrication of thin oxide films such as aluminum oxide and titanium oxide. Moreover, we reported the experimental demonstration of a high reflectivity of over 30% at a wavelength of 2.74 nm and an incident angle of 71.8° from the normal incidence using novel metal oxide multilayers consisting of titanium oxide and aluminum oxide fabricated by controlled growth by atomic layer deposition with sequential surface chemical reactions [1]. For high-power x-ray processing, crystalline multilayer mirrors might be more useful than those with amorphous layers. Therefore, the authors recently demonstrated the fabrication of novel oxide superlattice structures of crystalline $TiO_2$/ZnO on sapphire substrates for multilayer mirrors with high reflectivity at 2.74 nm [2, 3].

In the fabrication study, first of all, (001)-oriented wurtzite ZnO and (100)-oriented rutile $TiO_2$ films were grown on a (001)-oriented sapphire substrate by atomic layer epitaxy at a substrate temperature of 450 °C [4, 5]. These films were grown layer by layer owing to the self-limiting nature of surface chemical reaction. The ZnO films were grown using DEZ and $H_2O$ vapors at a constant growth rate of nearly 0.26 nm/cycle. The $TiO_2$ films were deposited using TCT and $H_2O$ at a constant growth rate of nearly 0.076 nm/cycle.

We fabricated a 10-bilayer $TiO_2$/ZnO multilayer mirror by atomic layer epitaxy at a substrate temperature of 450 °C [2, 3]. Figure 1 shows that the multilayer mirror achieved a high reflectivity of 29.4% at a wavelength of approximately 2.74 nm and a grazing angle of 2θ=10°. The FWHM of the experimentally obtained reflectivity at 2.74 nm was 0.041 nm, which corresponds to $\Delta\lambda/\lambda$=1.5%. The $TiO_2$/ZnO multilayer is expected to be useful for soft x-ray mirrors once further studies are conducted in terms of the growth rate, interface, surface roughness, and reactant vapors. Further reduction of the surface and interface roughness will lead to the fabrication of normal-incidence reflectors at the water-window wavelengths.

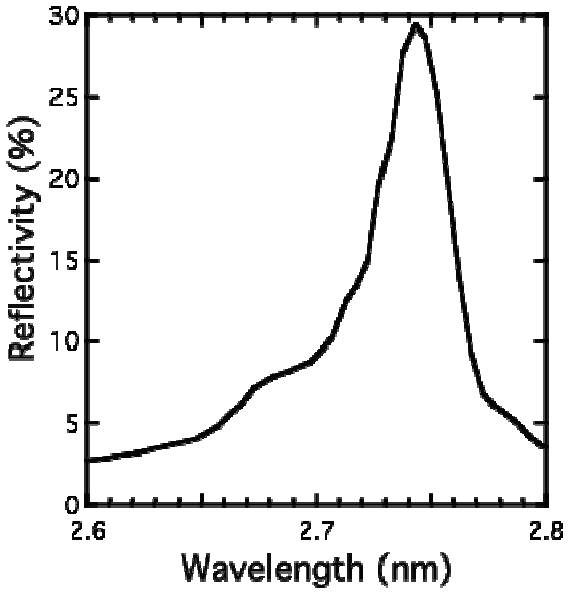


Fig. 1. Experimental reflectances of the ALE-grown 10-bilayer $TiO_2$/ZnO structure on a sapphire (0001) substrate at a wavelength of approximately 2.74 nm and a grazing angle of 2θ=10°.

[1] H. Kumagai, K. Toyoda, K. Kobayashi, M. Obara and Y. Iimura, Appl. Phys. Lett. **70** (1997) 2338.
[2] H. Kumagai, Y. Tanaka, M. Murata, Y. Masuda and T. Shinagawa, Journal of Physics: Condensed Matter **22** (2010) 474008 pp.1-7.
[3] H. Kumagai and Y. Yanagihara, Review of Laser Engineering **38** (2010) 976.
[4] H. Kumagai, Y. Masuda and T. Shinagawa, Journal of Crystal Growth **314** (2011) 146.
[5] H. Kumagai, Y. Masuda and T. Shinagawa, Materials Science and Engineering (2011) in press.

BL6U

# Band Alignment at CNT/SiC Interface Formed by Surface Decomposition

T. Maruyama[1], S. Sakakibara[1], H. Ito[1], H. Yamane[2], E. Shigemasa[2] and N. Kosugi[2]

[1]*Department of Materials Science and Engineering, Meijo University, Nagoya 468-8502, Japan*

[2]*Institute for Molecular Science, Okazaki 444-8585, Japan*

Carbon nanotube (CNT) growth by surface decomposition of SiC is a synthesis method for self-organized CNT films only by heating SiC single crystal at high temperature in a vacuum [1]. By this method, high density aligned zigzag-type CNTs can be produced perpendicular to the substrate surfaces (Fig. 1). Moreover, it has been demonstrated that grown CNTs are atomically bonded to SiC substrate [2]. This is a distinguished characteristic of this material, because there are some interlayers at the interface in other CNT/semiconductor heterojunctions. In this study, to clarify the electronic structure at the CNT/SiC interface, we performed the photoemission spectroscopy (PES) experiments.

CNT films formed by surface decomposition of 6H-SiC(000-1) face were used as samples. The current-voltage (I-V) measurement for CNT (~400 nm)/SiC heterojunction showed distinct rectifying behavior with the forward direction occurring at positively biased CNTs. For PES measurement, the samples with the CNT thickness of about several nm were also prepared to investigate the CNT/SiC interface. The PES measurement was carried out in a high-resolution angle-resolved PES system at BL6U. All PES spectra were measured at normal emission with the incident photon energy of 60 and 350 eV. The overall energy resolution was below 100 meV at room temperature (~300 K).

Figure 2 (a) shows photoemission spectrum near valence band maximum (VBM) of CNTs (~400 nm) with that of Au. The Fermi edge is observed in the spectrum of CNTs, indicating that they were metallic tubes.

The value of Schottky barrier height at the interface between metallic CNTs and SiC was evaluated by the energy difference between the C 1s core levels at the CNT/SiC interface (shown in Fig. 2 (b)) and the VBM to the core level separations in the CNT(~400nm)/SiC and SiC substrate samples, as described by

$$E_{SB} = E_g^{SiC} + \left(E_{C1s}^{SiC} - E_{VBM}^{SiC}\right) + \left(E_{C1s}^{CNT(CNT/SiC)} - E_{C1s}^{SiC(CNT/SiC)}\right) - E_{C1s}^{CNT}$$
$$= 3.0 + 280.87 + 1.76 - 284.22 = 1.41\ [eV]$$

where $E_i^S$ denotes the energy of feature $i$ in sample $s$, and the band gap of 6H-SiC, $E_g^{SiC}$, is 3.0 eV [3]. The obtained band alignment at the CNT/SiC interface is shown in Fig. 3. The Schottky barrier height at the CNT/SiC interface, 1.4 eV, is fairly high, compared with conventional metal/SiC Schottky barriers. Our result indicates that the band bending occurred at the interface, which might be induced by deep level traps.

This work was supported in part by the Joint Studies Program (2010) of the Institute for Molecular Science (IMS).

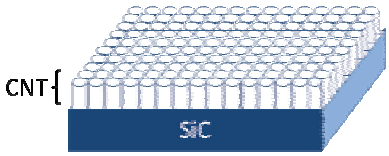


Fig. 1. Schematics of CNTs on SiC formed by surface decomposition.

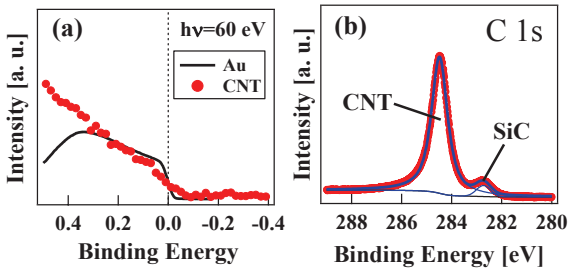


Fig. 2. Photoemission spectra of CNT (~400 nm)/SiC heterojunction: (a) valence band near the Fermi level (hν = 60 eV), (b) C 1s core level (hν = 350 eV).

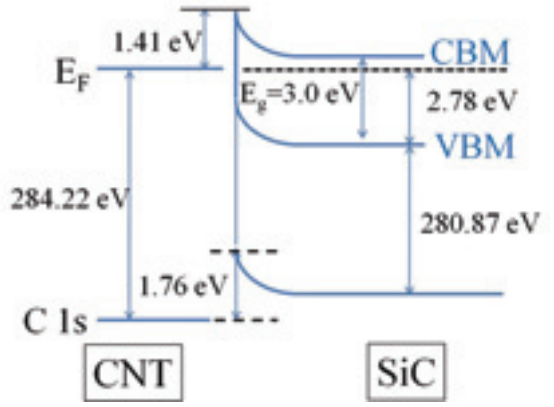


Fig. 3. Band alignment of CNT/SiC heterojunction.

[1] M. Kusunoki *et al.*, Appl. Phys. Lett. **77** (2000) 531.

[2] M. Kusunoki *et al.*, Chem. Phys. Lett. **366** (2002) 458.

[3] O. Madelung, Semiconductors: Data Handbook (Springer-Verlag) (2004) 61.

BL6B

# Far-Infrared Reflective Study of Alkali Niobate Ceramics

H. Matsudo, S. Koide, T. Nishi, I. Kagomiya and K. Kakimoto

*Graduate School of Engineering, Nagoya Institute of Technology Nagoya 466-8555, Japan*

## Introduction

Alkali niobate is one of the promising candidates of lead-free piezoelectric material. Li-doped $Na_{0.5}K_{0.5}NbO_3$ (LNKN) solid solution shows an excellent piezoelectric property of $d_{33}$=235 pC/N when the Li content is 6.0 mol% (L6). The phase transition of LNKN varies with Li content, and changes at room tempereature from orthorhombic to tetragonal at 5-7 mol% of Li content. However, LNKN undergoes the temperature-dependent successive structural phase transition. We have investigated such phase transition by using Raman scattering to clarify its origin and the related good piezoelectric property. Especially, the ferroelectric property recorded at room temperature was closely related to the frozen-modes of optical lattice vibration below room temperature. Therefore, the phonon behavior of L6 has been investigated more. In this study, IR reflectivity of LNKN ceramics was measured, and the effect of Li incorporation against the lattice vibration of LNKN was discussed.

## Experimental Procedure

The ceramic sample was synthesized by an ordinal solid-state reaction method. The surface of $Li_{0.06}(Na_{0.5}K_{0.5})_{0.94}NbO_3$ (L6) and $Na_{0.5}K_{0.5}NbO_3$ (NKN) ceramics were polished and used for IR reflective study.

Their reflectivity far-infrared spectra were obtained at 78 and 300 K using the beamline BL6B, then the spectra were corrected by using Michelson interferometer (Bruker, IFS66v) and synchrotron radiation source.

## Results and Discussion

Dielectric permittivity of L6 ceramics was calculated by Kramers-Kronig transform method. Any dielectric anomalies originated from structural phase transitions has not been detected below 273 K in the previous impedance analysis. However, an optical mode was disappeared during the heating step. Figure 1 shows the measured reflectance spectra of non-poled L6 ceramics at 110, 120, 130, 140 and 150 K. The optical mode was observed at 223 $cm^{-1}$ at temperatures below 150 K. This mode was not detected for NKN. Figure 2 shows the real part of permittivity of L6 ceramics and the fitting result. The strong peak of the mode could not fit well to a traditional oscillator model. A strong Li-O mode in LNKN seems to be correlated with the result, and we will investigate the further mode analysis for the poled-samples and single crystal.

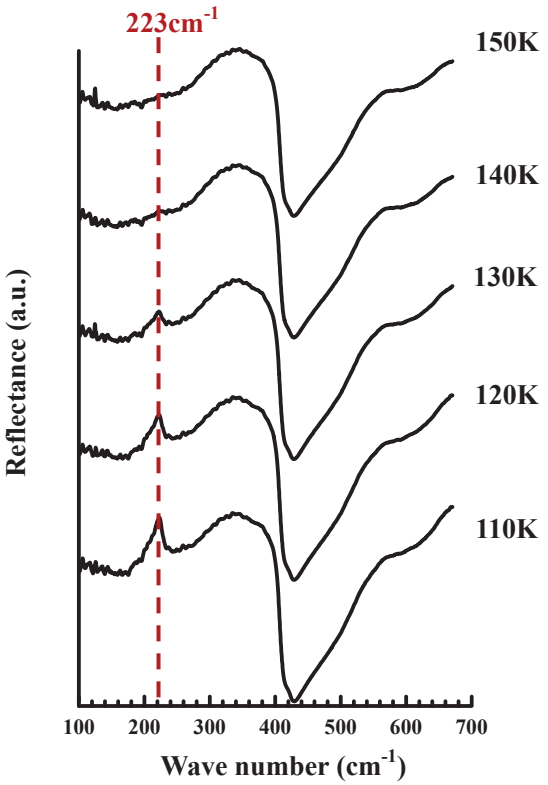


Fig. 1. Far-infrared reflectance spectra of L6 ceramics at 110, 120, 130, 140 and 150 K.

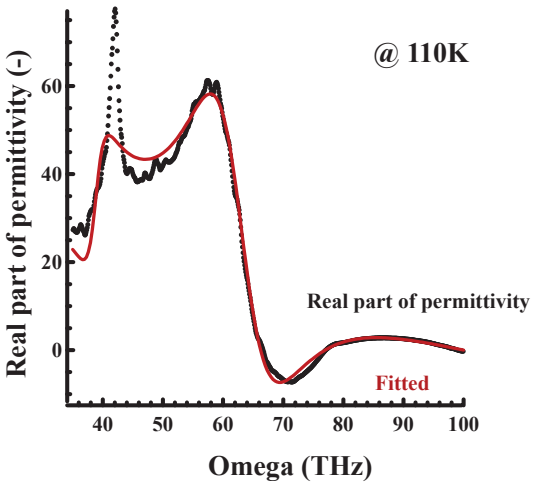


Fig. 2. Real part of permittivity of L6 ceramics at 110 K and the fitting result based on traditional oscillator model at 110 K.

## Acknowledgement

This research was supported by the Industrial Technology Research Grant Program in 2007 from the New Energy and Industrial Technology Development Organization (NEDO) of Japan.

BL7U

# Effects of Temperature Dependent Chemical Potential on Seebeck Coefficient of $TiS_2$

T. Takeuchi[1,2], A. Yamamoto[2] and K. Ogawa[2]
[1]*EcoTopia Science Institute, Nagoya University, Nagoya 464-8603, Japan*
[2]*Department of Crystalline Materials Science, Nagoya University, Nagoya 464-8603, Japan*

Temperature dependence of chemical potential was measured for the n-type $TiS_2$ thermoelectric material by means of angle resolved photoemission spectroscopy (ARPES), and compared with its measured Seebeck coefficient. The ARPES measurements were performed using 22 eV photon source and the MBS A1 analyzer located at the BL7U in the UVSOR at Okazaki, Japan.

Figures 1 (a) and (b) show typical example of ARPES intensity images obtained for the present sample at 15 K and 140 K along the momentum line crossing the M point. The intensity-peak varying with momentum is observable in the ARPES images. This experimentally revealed fact indicates that the quality of samples was good enough, and also that the electronic states in this sample are described with the Bloch states **k**. The presence of Bloch states **k** is responsible for the metallic electrical conduction observed for this sample. The energy shift of ARPES spectra with varying temperature is also observable for the present sample. This energy shift in ARPES spectra must be caused by the temperature dependence of chemical potential.

The chemical potential of n-type materials generally moves toward lower energy with increasing temperature. By considering that (a) the chemical potential of apparatus is kept constant regardless of the sample temperature and (b) the chemical potential observable in the photoemission spectra is pinned at the chemical potential of the apparatus, it is naturally understood that the photoemission spectrum at given temperature shifts towards the opposite energy direction of the chemical potential shift of samples. Indeed, the ARPES spectrum of the n-type $TiS_2$, in which the chemical potential is supposed to move towards lower energy, was moved towards higher energy with increasing temperature.

In order to quantitatively extract the temperature dependence of chemical potential from the measured ARPES spectra, the ridge in ARPES intensity, that indicates the energy–momentum dispersion, was plotted in Fig. 1 (c). From the determined energy-momentum dispersion, we identified that the chemical potential shift of −6 meV took place during the temperature increase from 15 K to 140 K [1].

The contribution of chemical potential to Seebeck coefficient was calculated from the measured value of chemical potential shift. We assumed here that the contribution of chemical potential to Seebeck coefficient is linearly varying with absolute temperature as it is described in the Sommerfeld theory, and mathematically transformed the equation $S_\mu(T)$; $(\mu(T)-\varepsilon_F)/(|e|T)$ into the following formula.

$$S_\mu(T) \approx T(\mu(T)-\mu(T_1))/(|e|(T^2-T_1^2)) \qquad (1)$$

The resulting value was $S_\mu(T) = -43$ $\mu$ V/K at 140 K, which exceeds 30 % of the measured value, $S$ (140 K) = −135 μV/K [1].

The present analysis clearly proved that the contribution of chemical potential to Seebeck coefficient is not negligibly small but considerably large. We have confirmed that this fact is also true for the $Bi_2Te_3$ and $Bi_2Se_3$ thermoelectric materials [2]. It is confidently argued, therefore, that the proper understanding of the relation between chemical potential and Seebeck coefficient should be required to develop a practical thermoelectric material possessing a large magnitude of Seebeck coefficient.

[1] T. Takeuchi, A. Yamamoto, K. Ogawa, Mater. Res. Soc. Symp. Proc. (2011), in press.
[2] A. Yamamoto, K. Ogawa, T. Takeuchi, Materials Transactions (2011), in press.

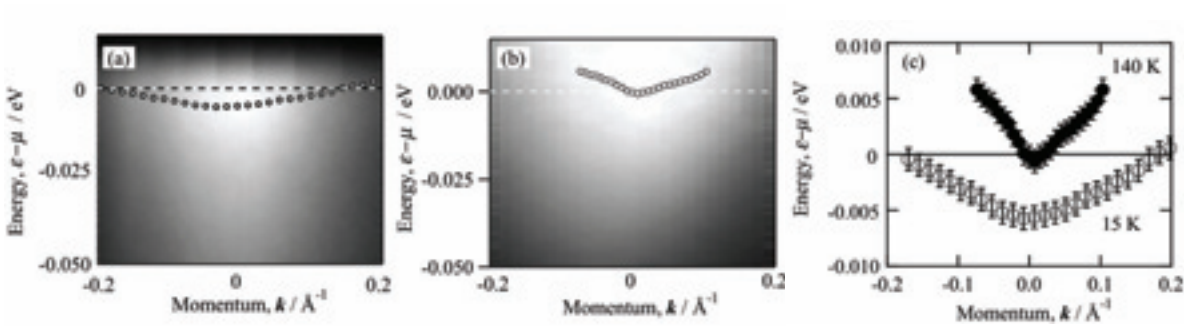


Fig. 1. ARPES intensity $I(\mathbf{k},e)$ of $TiS_2$ measured at (a) 15 K and (b) 140 K. In order to observe the states above $\mu$, the 140 K spectrum was divided by the Fermi-Dirac distribution function. The peak energy is plotted as a function of momentum in (c). The chemical potential shift of −6 meV was caused by the temperature increase from 15 K to 140 K [1].

BL7B

# Reflection Spectroscopy of 6FDA-Based Polyimide Films

H. Ito, N. Fujita, T. Yabumoto, S. Matsumoto and H. Matsumoto
*School of Science & Technology, Meiji University, Kawasaki 214-8571, Japan*

## Introduction

Photo-alignment is attracting attention as a method of fabricating the alignment layer in liquid crystal (LC) displays. In this method, a polyimide (PI) film is irradiated by linearly polarized ultraviolet light (LPUVL). In an alignment layer produced by this method, the LC molecules are oriented by a mechanism that is not understood.

We investigated the optical properties of PI films irradiated by LPUVL in the ultraviolet (UV) and vacuum ultraviolet (VUV) regions to examine the mechanism.

We used fluorine-containing PI that is expected to find wide application.

## Experimental

### *Materials*

We investigated the optical properties of PIs based on 2,2′-bis(3,4-dicarboxyphenyl)hexafluoro propane dianhydride (6FDA). Four types of phenylene were used as the diamine: 1,3-phenylene diamine (mPD), 4-methyl-1,3-phenylene diamine (MPD), 2,4,6-trimethyl-1,3-phenylene diamine (TMPD), and 2,3,5,6-tetramethyl-1,4-phenylene (TeMPD). They were synthesized at the Nagai lab, Meiji University [1]. Figure 1 shows their chemical structures.

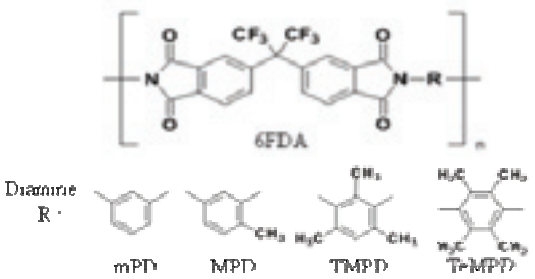


Fig. 1. Chemical structures of 6FDA-based PIs.

### *Sample preparation*

We dissolved the PIs with *N,N*-dimethylacetamide (DMAc). The PI films were prepared by spin coating on quartz substrates. The PI-coated substrates were baked at 100°C for 1 h. The film thicknesses were controlled to about 400 nm.

These PI films were irradiated by LPUVL from a 200 W Hg–Xe lamp. Linearly polarized light was obtained by reflection from a quartz plate at Brewster's angle. The degree of polarization was 99% at 254 nm. The irradiation intensity was about 700 μW/cm$^2$ at 254 nm. We irradiated the films with 8 J of LPUVL.

### *Reflection measurements*

UV and VUV reflectance spectra of the films were measured at up to 17 eV with a 3-m normal incident monochromator (grating: G2 and G3) at BL-7B of UVSOR. A silicon photodiode sensor was used to detect the reflected light.

## Results and Discussion

Figure 2 shows the UV and VUV reflectance spectra of the 6FDA-based PI films from 4.5 to 17 eV. The solid line indicates the reflectance before LPUVL irradiation, and the dotted line indicates the reflectance after 8 J of LPUVL irradiation.

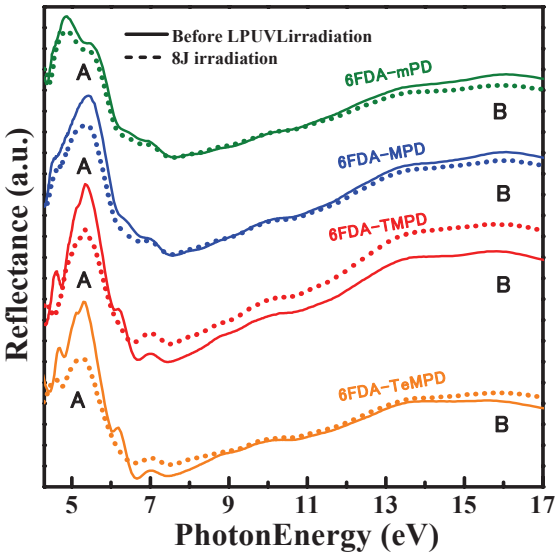


Fig. 2. Reflectance of 6FDA-based PIs.

The spectra of the PI films are fairly similar and consist of a prominent band group around 5.5 eV (the A band) and another broad band group (the B band) near 17 eV.

The appearance of the A band varied in the four spectra taken before LPUVL irradiation. The reason may be differences in the diamines.

A significant spectral change was observed after LPUVL irradiation of the 6FDA-TeMPD film. But the spectrum of the 6FDA-mPD film showed the least change after irradiation. This difference in the degree of spectral change implies that the methyl groups added to phenylene in the diamine affect the photo-alignment of PI films.

[1] S. Miyata *et al.*, J. of Appl. Polym. Sci. **107** (2008) 3933.

BL7B

# Auger-Free Luminescence Emitted from $A_2ZnCl_4$ (A = Cs, Rb) Crystals

A. Ohnishi[1], M. Saito[1], M. Kitaura[1], M. Sasaki[1], T. Kajitani[2] and M. Itoh[2]
[1]*Depeartment of Physics, Yamagata University, Yamagata 990-8560, Japan*
[2]*Department of Electrical and Electronic Engineering, Shinshu University, Nagano 380-8553, Japan*

The Auger-free luminescence (AFL) is a peculiar type of intrinsic luminescence in ionic crystals in which the valence excitation through a nonradiative Auger process is energetically forbidden. The AFL is characterized by a high quantum yield and a short lifetime of the order of ns. Therefore, it is very useful as the fast scintillator for high-energy physics, positron emission tomography and so on.

In the present work, we have investigated the luminescence of $A_2ZnCl_4$ (A = Cs, Rb) crystals under the outermost core excitation, in order to find the existence of AFL.

$A_2ZnCl_4$ (A = Cs, Rb) crystals were prepared by evaporating a stoichiometric mixture of solutions of CsCl or RbCl and $ZnCl_2$. Experiments were performed at the BL7B beamline of UVSOR. The emission spectra in this measurement were not corrected for the spectral dispersion. The excitation spectra were corrected for the spectral distribution of the light source.

When $Cs_2ZnCl_4$ was excited at 10 K at 21.4 eV, two luminescence bands appeared at 3.2 and 4.2 eV. The blue line of Fig. 1 shows the excitation spectrum for the 4.2 eV band. The excitation spectrum for the 3.2 eV band was practically the same as that for the 4.2 eV band. For reference, the reflection spectrum measured for the cleaved surface of $Cs_2ZnCl_4$ is also shown by the red line. Sharp peak at 7.3 eV is assigned to the $n$ = 1 exciton absorption, which is due to the transition from the Cl 3$p$ valence band to the conduction band. Sharp peaks at 13.2 and 13.9 eV may be core exciton bands due to the transitions from the outermost core band to the conduction band.

The excitation spectrum rises at around 13.5 eV as the photon energy is increased. This threshold energy corresponds almost to the transition energy between the outermost core band and the conduction band, and thus both of the 4.15 eV and 3.31 eV bands are supposed to be the AFL bands due to the radiative recombination between a valence electron and an outermost core hole. It is noteworthy that the threshold energy of the AFL is slightly higher than the lowest-energy core exciton band at 13.2 eV. This fact suggests that core excitons decay nonradiatively through Auger-electron emission.

Luminescence decay measurements were also performed using a time-correlated single-photon counting technique under the single bunch operation. It was proved that, at 10 K, the 4.15 eV and 3.31 eV bands are composed of a fast decay component with the lifetime of about 1.8 ns.

In $Rb_2ZnCl_4$ crystal, two AFL bands peaking at 2.8 and 4.3 eV were observed at 10 K under excitation at 21.4 eV. In Fig. 2, excitation (blue) and reflection (red) spectra of $Rb_2ZnCl_4$ are shown. The excitation spectra for the 2.8 and 4.3 eV bands were the same. Sharp peaks at 7.3 and 16.5 eV in the reflection spectrum is assigned to the n = 1 exciton and core exciton absorption bands, respectively. From the excitation spectrum, it turns out that both bands are stimulated with photons above about 14 eV. This result suggests that the 2.8 and 4.3 eV bands are the AFL bands in $Rb_2ZnCl_4$. However, it should be noticed that the threshold energy is located at the energy lower than the core exciton peaks. The reason for such a disagreement is under investigation now.

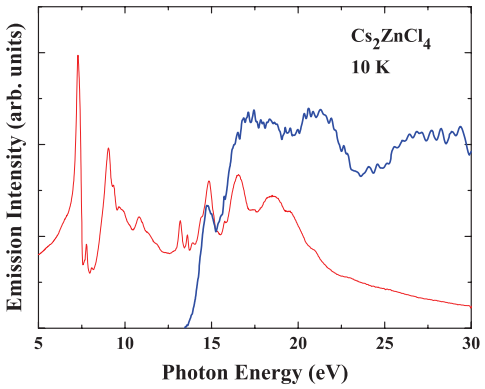


Fig. 1. Excitation spectrum at 10 K for the 4.2 eV band in $Cs_2ZnCl_4$ (blue line). Reflection spectrum (red line) is also shown for reference.

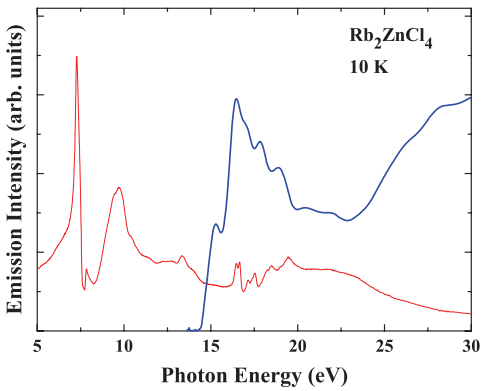


Fig. 2. Excitation spectrum at 10 K for the 4.3 eV band in $Rb_2ZnCl_4$ (blue line). For reference, reflection spectrum is also shown by a red line.

BL8B

# Electronic Structure of Delocalized Singlet Biradical $Ph_2$-IDPL Solid Film

K. Kanai[1], Y. Noda[2], K. Kato[2], T. Kubo[3], K. Nakasuji[4] and K. Seki[2]

[1] *Department of Physics, Faculty of Science and Technology, Tokyo University of Science, Noda 278-8510, Japan*

[2] *Department of Chemistry, Graduate School of Science, Nagoya University Nagoya 464-8602, Japan*

[3] *Department of Chemistry, Graduate School of Science, Osaka University, Osaka 560-0043, Japan*

[4] *Fukui University of Technology, Fukui 910-8505, Japan*

Recently, Kubo *et al.* have successfully isolated a biradical hydrocarbon, diphenyl derivative of s-indacenodiphenalene ($Ph_2$-IDPL) which possesses a relatively small HOMO-LUMO gap $E_g$ and strong intermolecular interactions [1]. The partial occupation of the LUMO is thought to contribute to stabilization of the intermolecular interaction, leading to intermolecular covalency. Thus, a strong intermolecular interaction is characteristic of singlet biradicals.

In this work, the electronic structure of a $Ph_2$-IDPL film has been investigated. A small $E_g$ compared with that of typical $\pi$-conjugated small molecules was observed even for the amorphous film of $Ph_2$-IDPL. This result indicates that the small $E_g$ is an important characteristic of the singlet biradical electronic structure. Moreover, the photon energy dependence of ultraviolet photoemission spectra shows that the stacked $Ph_2$-IDPL molecular chain in the polycrystalline film develops an energy band structure in the direction of the surface normal of the film. The intermolecular covalency therefore evolves into the quasi one-dimensional energy band along the molecular stacking direction.

The UPS measurements were performed at the BL8B of the UVSOR.

Figure 1 shows UPS and IPES spectra of $Ph_2$-IDPL amorphous film on graphite substrate. The simulated spectra for the monomer well explain the observed spectra over the entire energy range. Since strong intermolecular coupling among the molecules is expected to significantly alter its electronic structure, these results clearly show that this $Ph_2$-IDPL film on graphite is composed of the monomers. Notably, the observed $E_g$ is rather small. From the results shown in Fig. 1, $E_g$ is about 1.2 eV, which is smaller than those of many other typical $\pi$-conjugated molecules.

Figure 2 shows the UPS and IPES spectra of $Ph_2$-IDPL crystal and the polycrystalline film. The film spectra differ from the spectra for a monomer. In particular, the electronic structure of the film around $E_F$ produces broader spectral features compared to the monomer spectra. The UPS spectrum of the film closely resembles that of the crystal. The $E_g$ for the polycrystalline film was estimated to be 0.84 eV. These results well explains the previously reported ambipolar field effects of amorphous $Ph_2$-IDPL film

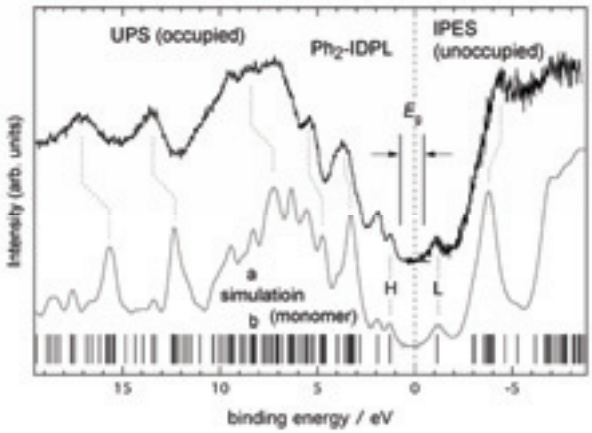


Fig. 1. UPS and IPES spectra of $Ph_2$-IDPL film on graphite. Simulated spectra labeled "a" were calculated by the DFT method for monomer.

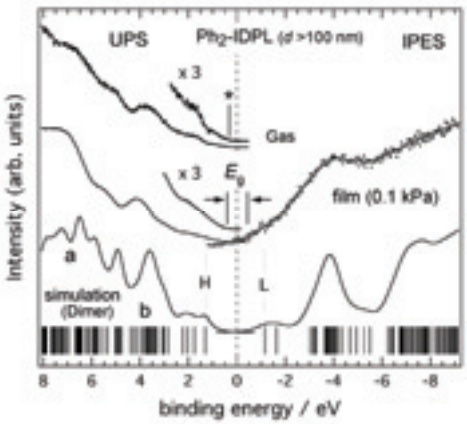


Fig. 2. UPS and IPES spectra of $Ph_2$-IDPL film on graphite and simulated spectra for the dimer.

by Chikamatsu *et al.* [2]. The small $E_g$ would result in a small injection barrier both for electrons and holes at the electrode interface. The extremely small $E_g$ observed in the polycrystalline $Ph_2$-IDPL film is possibly caused by strong intermolecular coupling.

[1] T. Kubo *et al.*, Angew. Chem. Int. Ed. **44** (2005) 6564.

[2] M. Chikamatsu *et al.*, Appl. Phys. Lett. **91** (2007) 043506.

BL8B

# Interface Electronic Structures of a High Performance Organic Planar Hetero-junction Solar Cell

Y. Nakayama[1], J. Wagner[2], Y. Tanaka[3], S. Machida[3], T. Nishi[1,4], A. Opitz[2], W. Brütting[2] and H. Ishii[1,3]

[1]*Center for Frontier Science, Chiba University, Chiba 263-8522, Japan*
[2]*Institute of Physics, University of Augsburg, Augsburg 86135, Germany*
[3]*Graduate School of Advanced Integration Science, Chiba University, Chiba 263-8522, Japan*
[4]*UVSOR Facility, Institute for Molecular Science, Okazaki 444-8585, Japan*

Organic photovoltaics (OPVs) are expected as next generation power conversion devices complementary to conventional Si-based solar cells. For OPVs, a bulk hetero-junction concept is generally adopted to redeem small exciton diffusion length, nevertheless this concept also has disadvantages (e.g. spoiled effective mobility $\mu_{eff}$) that depress the power conversion efficiency. A planar hetero-junction (PHJ) OPV based on diindenoperylene (DIP) and $C_{60}$ was recently reported to reveal high performance [1]. DIP has to be deposited on a heated hole injection layer (HIL) to achieve high efficiency. The origin(s) of the improved performance, which may be attributed to a reduced interface energy barrier and/or enhanced bulk $\mu_{eff}$ of DIP, have not been clarified yet. In this study, we determined the interface electronic structures of the DIP-$C_{60}$ based high performance PHJ-OPV.

EDOT:PSS substrates were prepared by a method described in Ref. [1] in nitrogen atmosphere. The work function of the substrate varied in the range of 4.9 ± 0.2 eV. DIP was deposited (ca. 0.05 nm/s) onto the polymer substrates at ca. 100 °C in high vacuum. Note that heating of the polymer up to the deposition temperature significantly increased the work function [Fig. 1 (a)]. $C_{60}$ was deposited (ca. 0.02 nm/s) onto a DIP thin film at RT. All PES spectra were taken with the photon energy of 40 eV at BL8B in UVSOR. For the organic films of 1.5 nm or thicker, sample bias of +5 V was applied in order to avoid sample charging.

Figure 1 shows the UPS secondary electron cutoff (SECO) and spectra of a PEDOT:PSS substrate and DIP overlayers. The onset of the highest occupied molecular orbital (HOMO) of DIP ($\Phi_h$) appeared at 0.2 eV from the Fermi level ($E_F$). This value is apparently smaller than the literature (0.45 eV [1]) of DIP films deposited at RT. In addition, a negative vacuum level shift ($\Delta$) is evinced by SECO, which is also strikingly in contrast to the RT deposition case.

The HOMO level offset ($\Delta E$) at the $C_{60}$-DIP interface is estimated to be 1.0 eV as shown in Fig. 2. Slightly positive $\Delta$ was revealed at this interface. The energy level diagram of the topical OPV cell is shown in Fig. 2 (d). Despite aforementioned HOMO energy difference, $\Delta E$ is identical to that of the interface formed on DIP deposited at RT (1.05 eV [1]). The reduced $\Phi_h$ by high temperature DIP deposition should be a reason of improved OPV performance.

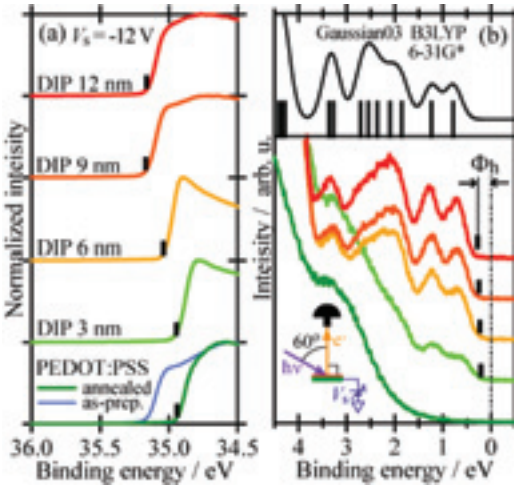


Fig. 1. (a) SECO and (b) UPS of DIP deposited on a heated PEDOT:PSS substrate. A simulated density-of-state curve of DIP is shown in the upper panel of (b).

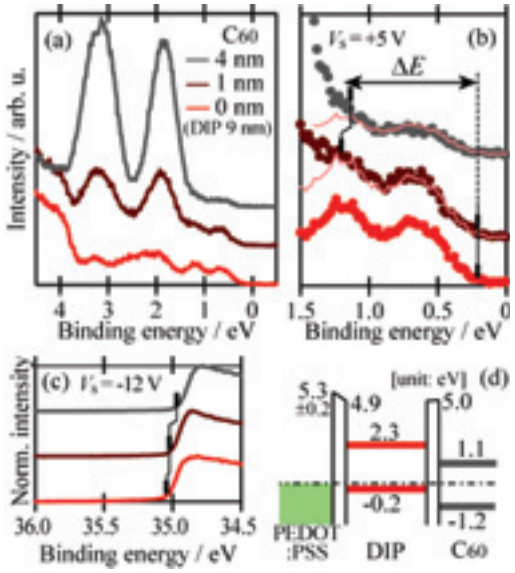


Fig. 2. (a) UPS spectra of $C_{60}$ deposited on DIP(9 nm) /PEDOT:PSS. (b) Magnified spectra of (a). Thin red lines indicate hypothetical DIP contribution. (c) SECO spectra of $C_{60}$ on DIP/PEDOT:PSS. (d) An energy level diagram of the hetero-interfaces in the DIP-$C_{60}$ based high performance PHJ-OPV [1]. The numbers represent the energy with respect to $E_F$.

[1] J. Wagner *et al.*, Adv. Funct. Mater. **20** (2010) 4295.

BL8B

# Electronic Structures of Room Temperature Ionic Liquids Studied by UPS and IPES

T. Sato[1], T. Iwahashi[1,2], Y. Sakai[1], K. Kanai[3], T. Nishi[4] and Y. Ouchi[1]

[1] *Department of Chemistry, Nagoya University, Nagoya 464-8602, Japan*
[2] *Venture Business Laboratory (VBL), Nagoya University, Nagoya 464-8601, Japan*
[3] *Faculty of Science and Technology, Department of Physics, Tokyo University of Science, Chiba 278-8510, Japan*
[4] *UVSOR Facility, Institute for Molecular Science, Okazaki 444-8585, Japan*

Room temperature ionic liquids (RTILs) are salts in a liquid phase at ambient temperature and pressure, and have attracted much attention due to their unique nature of nonvolatility, high conductivity, and wide electrochemical window. Recently, RTILs are utilized as a potential gate material for organic field effect transistors as well as capacitors, fuel cells, organic photovoltaic cells, and Li-ion batteries. In such applications, electronic structure, such as HOMO and LUMO levels, of RTIL strongly affects the performance of the devices, and hence understanding of the electronic structures of RTILs should be a key issue for further development of such potential applications.

In this brief report, we examined the HOMO and LUMO levels and the energy gaps of the TFSA RTILs with cations of 1-ethyl-3-methylimidazolium ($[emim]^+$), 1-propyl-1-methyl pyrrolidinium ($[P13]^+$), 1-butyl- 1-methyl pyrrolidinium ($[P14]^+$), 1-propyl-1-methylpiperidinium ($[PP14]^+$), *N,N,N*-trimethyl propylammonium ($[TMPA]^+$), and $[DEME]^+$ cations by UPS and IPES. UPS measurements were carried out at the beamline BL8B2 of UVSOR facility at Institute for Molecular Science. IPES measurements were conducted at Nagoya University. The samples were prepared by putting one droplet of RTIL on scratched Au substrates. All measurements were performed under ultra-high vacuum condition of $2 \times 10^{-8} \sim 1 \times 10^{-7}$ Pa.

Figure 1 shows the UPS and IPES spectra of the TFSA RTILs with respect to the Fermi level of Au. The results for $[DEME]BF_4$ are also shown as a reference. As is seen in Fig. 1, the HOMO and LUMO levels of each RTIL differ from those of the isolated ions estimated from the *ab initio* calculations,[1)] and these energy shifts are toward the lower and higher energies for the cation and the anion, respectively. This energy shift is understood as a contribution of Madelung energy which stabilizes and destabilizes the orbital energies of the anion and the cation, respectively. On the other hand, we found that the energy gaps of the quaternary ammonium-based RTILs are wider with shifting the HOMO and LUMO levels higher and lower binding energy side, respectively, relative to those of [emim]TFSA as shown in Fig. 1. It is noteworthy that not only the energy gap but also the HOMO and LUMO levels are almost the same for the quaternary ammonium-based RTILs other than [DEME]TFSA even if the calculated energy gap has some differences for each cation. Considering that the calculated energy gap of the TFSA anion is much narrower than that of the quaternary ammonium-based cations except the $[DEME]^+$ cation, we can propose that both the HOMO and LUMO levels of the ammonium-based RTILs examined in this study, except [DEME]TFSA, is attributed to the TFSA anion. The observed energy gaps of the quaternary ammonium-based RTILs without methoxy group are also ~2 eV wider than the calculated gap of the TFSA anion similarly to the case of [emim]TFSA. The energy gap broadening of ~2 eV seems to be a condensed state effect for the TFSA RTILs.

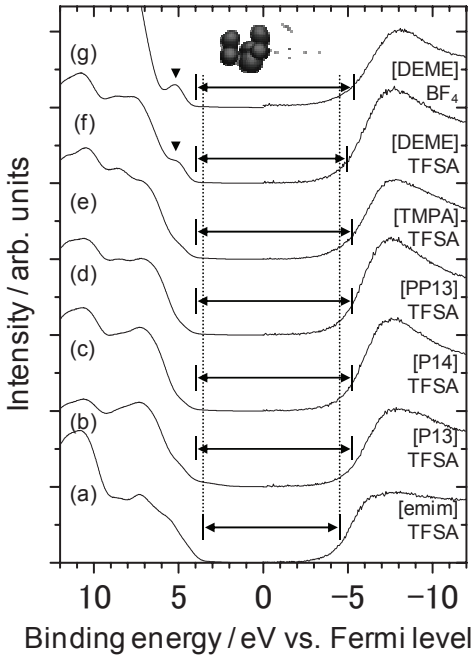


Fig. 1. UPS and IPES spectra of (a) [emim]TFSA, (b) [P13]TFSA, (c) [P14]TFSA, (c) [PP13]TFSA, (e) [TMPA]TFSA, (f) [DEME]TFSA, and (g) $[DEME]BF_4$. The abscissa is set the Fermi level of the Au substrate as zero. Inset shows the MO pattern of HOMO of $[DEME]^+$ cation. The triangles on the UPS spectra represent the peaks originating from O 2p of $[DEME]^+$ cation.

[1] K. Kanai *et al.*, J. Electron Spectrosc. Relat. Phenom. **174** (2009) 110.

BL8B

# Experimental Evidence of Acceptor-Like Levels in $SrGa_2S_4:Eu^{2+}$ Phosphor Thin-Films

Y. Suzuki[1], M. Kitaura[1], S. Tanaka[2], H. Kominami[3], K. Hara[3], A. Ohnishi[1] and M. Sasaki[1]
[1]*Faculty of Science, Yamagata University, Yamagata 990-8560, Japan*
[2]*Interdisciplinary Faculty of Science and Engineering, Shimane University, Matsue 690-8504, Japan*
[3]*Research Institute of Electronics, Shizuoka University, Hamamatsu 432-8011, Japan*

The type of charge carrier in narrow-gap semiconductors can be artificially controlled by the addition of impurities. The exchange of carrier type between electron and holes is challenge in wide-gap semiconductors with ionic character, because the *p*-type conduction due to holes is hard to occur due to the large effective mass and strong phonon coupling. Therefore, there have been few reports that succeeded the carrier type exchange in the wide-gap semiconductors. Recently, Tanaka *et al*. have reported that the hot carrier type in inorganic electroluminescence (EL) thin-film devices is exchangeable for different rare-earth ion doping [1]. Strontium thiogallate ($SrGa_2S_4$) is also one of the host materials showing such carrier type exchange. This material has the feature of *n*-type in $Ce^{3+}$-doping. The carrier type is changed to *p*-type in $Eu^{2+}$-doping. Judging from the practical sense mentioned above, these results are to be very surprising. On the other hand, there are ambiguous points on the fundamental physic of such *p*-type conduction, *e.g*., the presence of acceptor-like levels and the contact type at the interface between phosphor and metal electrode thin-films. The elucidation of these points is our main purpose: hence, ultraviolet photoelectron spectroscopy (UPS) experiment was carried out.

$Eu^{2+}$-doped $SrGa_2S_4$ thin-films were deposited on quartz substrates heated at 200 °C using electron beam sources. The concentration of $Eu^{2+}$ ions was set to be 2 mol% in the preparation. The thickness was adjusted to be 100 nm using quartz oscillators. The as-deposited thin-films were annealed at 850 °C in the $H_2S$+Ar gas mixture for 30 minutes, in order to supply with sulfur. The composition and crystalinity of $SrGa_2S_4:Eu^{2+}$ thin-films were checked by X-ray diffraction measurement. In UPS experiment, the surface was cleaned in vacuum with $Ar^+$ ion gun. An appearance of the clean surface was judged from the peak energy and spectral shape of the Ga-3*d* peak.

Figure 1 (a) shows the typical UPS spectrum of $SrGa_2S_4;Eu^{2+}$ thin-films at room temperature under excitation with photons at 18 eV. The absolute binding energy was determined by referring to the Fermi level of tantalum plates for the fixing of samples. In Fig. 1 (a), a prominent band appears around 5.0 eV. This band is ascribed to the valence band dominated by S-3*p* orbitals [2]. As shown in Fig. 1 (b), this band starts at $E_{th}$=0.86 eV. The fundamental absorption edge of $SrGa_2S_4$ is located at 4.0 eV,

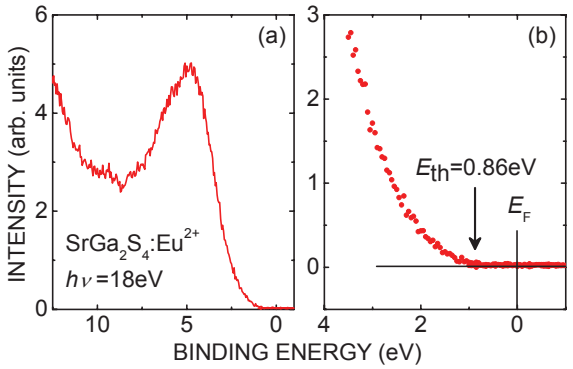


Fig. 1. UPS spectrum of $SrGa_2S_4:Eu^{2+}$ thin-films at room temperature under excitation with photons at 18 eV: (a) Valence band region and (b) near-Fermi level region.

according to the absorption spectrum at room temperature [3]. We suppose that the fundamental edge is due to the band-to-band transition, because no exciton absorption peaks were found in the reflection spectrum at room temperature. In this case, the threshold energy for the valence band is expected to be 2.0 eV, higher than the value of $E_{th}$. This result can be explained by considering that acceptor-like levels are on the valence band. Therefore, our experimental results are adopted as one of the evidence supporting that holes are dominant charge carrier in the $SrGa_2S_4:Eu^{2+}$ thin film.

UPS experiment allows us to know not only the electronic structure but also the physical constants characteristics of materials. We determined the ionization potential of $SrGa_2S_4:Eu^{2+}$ to be 4.96 eV. This value is higher than the work functions of metals except gold [4]. From this fact, it is suggested that the interface between $SrGa_2S_4:Eu^{2+}$ and metal electrode thin-films shows a tendency to form the Shottky-type barrier for hole conduction. The Shottky-type barrier may also involve the *p*-type conduction in the $SrGa_2S_4:Eu^{2+}$ thin-film.

[1] K. Tanaka and S. Okamoto, Appl. Phys. Lett. **89** (2006) 203508.
[2] M. Kitaura *et al*., UVSOR Activity Report **37** (2010) 137.
[3] C. Chartier *et al*., Electrochem. Solid-State Lett. **9** (2006) G53.
[4] H. B. Michaelson, J. Appl. Phys. **48** (1977) 4729.

BL8B

# Photoinduced Shift of the Photoelectron Spectra at the Zn-Phthalocyanine/$C_{60}$ Interface

S. Tanaka, K. Fukuzawa and I. Hiromitsu
*Interdisciplinary Faculty of Science and Engineering, Shimane University, Matsue 690-8504, Japan*

The electronic structure of the organic/organic and the organic/electrode interface of the organic electronics devices, such as organic light emitting diode, organic solar cell, and organic thin film transistor, has attracted much interest since it affects the performance of these devices [1]. For example, the authors have recently reported that the lithium-phthalocyanine thin film on indium-tin oxide (ITO) improves the device performance of the organic solar cell. This improvement was caused by the formation of the advantageous electronic structure for the hole extraction at the ITO/organic layer [2, 3]. It is widely accepted that the electronic structure of the organic layer in the devices can be inferred from the photoelectron spectra of the organic thin films. The photoelectron spectroscopy is a powerful tool for the estimation of the electronic structure of the samples. Thus, the photoelectron spectroscopy under the solar light irradiation can be useful to understand the electronic structure of the organic solar cells under the working condition. In the present study, we focused on the electronic structure of a donor/acceptor (DA) heterojunction of the organic solar cells. As a typical DA interface of the organic solar cell, the Zn-phthalocyanine (ZnPc)/$C_{60}$ interface was studied.

The photoelectron spectra were measured as a function of the thickness of the organic layer on an ITO substrate *in situ*. For the observation of the photoinduced effect on the electronic structure, the photoelectron spectra under the light irradiation were compared with that under dark. A solar simulator was used as the light source for the irradiation. The simulated airmass 1.5 solar illumination was exposed to the sample in a vacuum chamber through a viewport. The distance from the viewport to the sample was approximately 30 cm. All the photoelectron measurements were carried out with a photon energy of 40 eV at room temperature. The overall energy resolution was approximately 0.2 eV.
Figure 1 shows the photoelectron spectra of the $C_{60}$ (1 nm) layer on the ZnPc (15 nm) layer. The abscissa indicates the kinetic energy of photoelectron. The red dots and the black dots represent the photoelectron signals with and without the light irradiation, respectively. The peak at around 33.8 eV is the highest occupied molecular orbital (HOMO) of ZnPc. The HOMO peak position was shifted toward higher kinetic energies approximately 0.06 eV under the light irradiation compared with the HOMO peak under dark. In contrast, no significant shift was observed on the HOMO peak position of the ZnPc film without the $C_{60}$ over layer (not shown). The photoinduced shift showed dependences both on the light intensity and on the thickness of the $C_{60}$ layer.

In general, there are several possibilities for the origin of the spectrum shift: the degradation of the molecules, the charging up of the sample, the thermal effect, and the photoinduced charge redistribution. We have considered that the shift was caused by the photoinduced charge redistribution at the ZnPc/$C_{60}$ interface from the following reasons. The degradation of the molecules should cause nonreversible changes on the photoelectron spectrum, however, the present shift was observed reversibly. The charging up is also excluded, since the charging up would cause a shift toward the lower kinetic energies and deform the spectral shape. Although the slight increase of the temperature of the substrate was observed while the light irradiation, the effect of the temperature on the photoelectron spectra is empirically negligible in the present temperature range. Hence, the shift of the HOMO peak can be attributed to the photoinduced effects on the charge redistribution at the DA interface. These preliminary results indicate that the photoelectron spectroscopy under the light irradiation is a valuable method to investigate the electronic structure of the organic solar cell system under the working conditions.

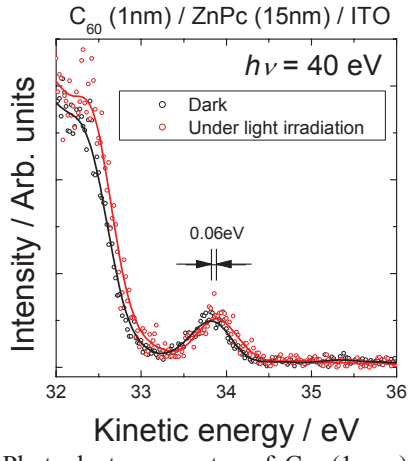


Fig. 1. Photoelectron spectra of $C_{60}$ (1 nm) / ZnPc (15 nm) on the ITO substrate with (red) and without (black) the light irradiation.

[1] H. Ishii *et al.*, Adv. Mater. **11** (1999) 605.
[2] S. Tanaka *et al.*, UVSOR Activity Report **37** (2009) 80.
[3] S. Tanaka *et al.*, Appl. Phys. Lett. **97** (2010) 253306.

BL8B, BL4B

# Identification of Catalytic Active and Inactive Species in Nitrogen Doped $TiO_2$ Photocatalyst by N K-edge XAFS Analysis

T. Yoshida[1], S. Muto[2] and E. Kuda[2]

[1]*EcoTopia Science Institute, Nagoya University, Nagoya 464-8603, Japan*
[2]*Department of Materials, Physics and Energy Engineering, Nagoya University, Nagoya 464-8603, Japan*

## Introduction

In the field of catalytic chemistry, a specific function in a solid catalyst crucially depends on the chemical state of a specific active component (active site). In this context X-ray absorption fine structure (XAFS) is expected as one of the most powerful techniques for chemical state analysis of the active site, because it provides information on the local structure and electronic states around the specific element of interest. In the present study, a sophisticated combination of XAFS and a theoretical calculation method allows us identification of photocatalytic active and inactive species in nitrogen doped $TiO_2$ catalysts.

## Experimental

The samples used in this study were $TiO_2$ (1 0 0) single crystals (5 x 5 x 0.5 $mm^3$), supplied by Furuuchi Kagaku, Japan. Mass analyzed 100 keV $N_2^+$ ions (50 keV/ $N^+$ ion) were injected into the samples at room temperature, perpendicular to the sample surface. The $N^+$ fluence ranged from 1 to 5 x $10^{21}$ $m^{-2}$. After the ion implantation, parts of the samples were heat-treated at 573 K for 2 hours in air.

A typical photocatalytic experiment consisted of placing the $N^+$-implanted sample in 0.5 ml of aqueous methylene-blue (MB) solution (9.8 μmol/L) and subsequent exposure to visible-light using a 15 W Xe lamp with a cut filter for $\lambda > 430$ nm.

N K-edge XANES spectra of the $N^+$-implanted $TiO_2$ samples were measured at the BL8B&4B station of UVSOR-II at the Institute for Molecular Science, Okazaki, Japan. Data were recorded at room temperature in total electron yield mode, and the X-ray energy dependence of the N Auger electron yield was monitored.

## Results and Discussion

The photocatalytic activity reached its maximum at a fluence of 3 x $10^{21}$ $m^{-2}$ and then decreased with the fluence. The sample implanted at a fluence of 5 x $10^{21}$ $m^{-2}$ followed by heat-treatment at 573 K was almost photocatalytically-inactive under visible-light irradiation.

Figure 1 shows N K-edge XANES spectra of the $N^+$-implanted $TiO_2$ samples, a TiN powder and theoretical spectra of several structure models.

Common XANES features in Fig. 1 (a) and (c) suggest that N in the sample implanted by 3 x $10^{21}$ $m^{-2}$ (highest active photocatalyst: H-cat) is in a chemical environment similar to that in TiN. More thorough observation suggested that double-peak around 400 eV in Fig. 1 (c) shifted to the lower energy side compared with that of TiN, which was well reproduced by the theoretical prediction using FEFF code when N occupies one of the O sites of $TiO_2$ [Fig. 1 (d)]. On the other hand, the XANES spectrum of the sample implanted with the $N^+$ fluence of 5 x $10^{21}$ $m^{-2}$ followed by heat-treatment (almost inactive to visible-light : I-cat) shows a distinct single peak around 401 eV [Fig. 1 (e)]. This feature of the XANES spectrum was succesffuly reproduced by theoretical simulations based on the model where an O atom in $TiO_2$ was replaced by $NO_2$ [Fig. 1 (f)].

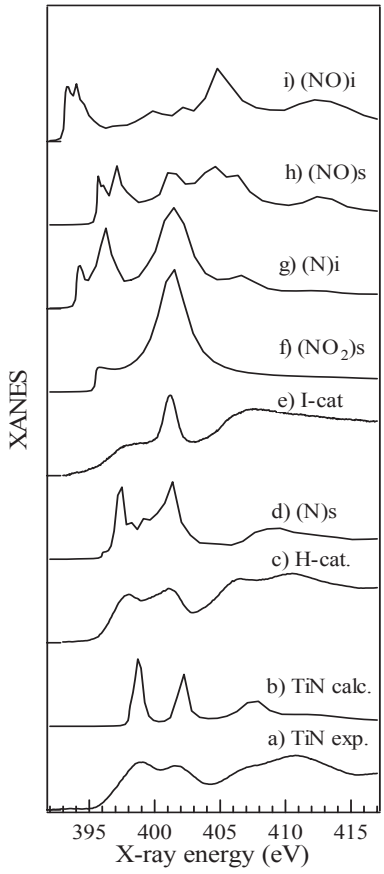


Fig. 1. N K-edge XANES spectra of (a) TiN crystal, (c) the sample $N^+$-implanted with 3 x $10^{21}$ $m^{-2}$, (e) that with 5 x $10^{21}$ $m^{-2}$ followed by heating at 573 K for 2 h, and theoretical spectra of structure models for (b) TiN, (d) substitutional N-doping, (e) substitutional $NO_2$-doping, (g) interstitial N-doping, (h) substitutional NO-doping and (i) interstitial NO-doping.